Politecnico di Torino

Department of Mechanical and Aerospace Engineering

Master's Degree Course in Aerospace Engineering

Master's Degree Thesis

Pollutant and GHG emissions predictions of high-speed aircraft using LH_2

Main supervisor:
Prof.ssa Nicole Viola

Candidate:
Dal Bo Lorenzo

Other supervisors:
Prof.ssa Roberta Fusaro
Dr. Guido Saccone

Academic year 2021/22
Torino

Abstract

In recent years, the global commitment aimed at reducing the environmental impact of all human activities, is increasingly growing: it is therefore in this perspective of farsightedness that aeronautical activity must evolve, setting as an objective of equal importance the satisfaction of users and also a limitation of the direct and indirect emission of pollutants. While on the one hand technological innovation has led to the development of innovations in propulsive terms, thus allowing to plan and design commercial flights at hypersonic speeds, on the other hand it has made it necessary to create new techniques for analyzing and forecasting pollutant and greenhouse gas emissions right from the conceptual design phase. In this context, engines such as the air turbo rocket, an innovative combined cycle air-breathing propulsion system, are developed. This thesis work has as first objective the in-depth analysis of the ATR cycle, deepening the development of a tool that allows to describe its performance accurately in various flight regimes. The results will be validated through a comparison with a propulsive database produced by the von Kàrmàn Institute for Fluid Dynamics through advanced analysis tools.

Once an effective propulsion model has been defined, the work will continue investigating the effective applicability, to an ATR system, of the emission prediction method known as $P_3 - T_3$, laying the foundations for its adaptation to hydrogen combined cycle hypersonic engines.

This thesis work was carried out in the context of a scientific collaboration between the Polytechnic of Turin and the Centro Italiano Ricerche Aerospaziali CIRA S.c.p.a., in the framework of the European projects STRATOFLY and MORE and LESS.

Abstract

In questi anni si sta assistendo ad un crescente impegno globale mirato alla riduzione dell'impatto ambientale di tutte le attività umane: è verso questa prospettiva di lungimiranza che l'attività aeronautica deve evolversi, imponendosi come un obiettivo di uguale importanza la soddisfazione dell'utenza e la diretta ed indiretta riduzione dell'emissione di inquinanti. Mentre da un lato l'innovazione tecnologica ha portato allo sviluppo di novità in termini propulsivi, rendendo i regimi di velocità ipersonici accessibili a pianificazioni di volo commerciale, dall'altro canto ha reso necessario sviluppare nuove tecniche per analizzare e predire l'emissioni di gas serra ed inquinanti già dalla fase di conceptual design. In questo contesto, si sono sviluppati motori come l'ATR, un innovativo sistema propulsivo combinato di tipo air-breathing. Questo lavoro di tesi ha come primo obiettivo una profonda anlisi del ciclo termodinamico dell'ATR, approfondendo lo sviluppo di un modello che permetta di descriverne le performances propulsive in diversi regimi di volo. I risultati saranno validati attraverso un confronto con un database propulsivo prodotto dal von Kàrmàn Institute for Fluid Dynamics attraverso strumenti di analisi avanzata.

Dopo aver sviluppato un modello propulsivo efficacie, il lavoro procederà investigando l'effettiva applicabilità dei metodi analitici di predizionie degli inquinanti su motori a ciclo combinato come l'ATR, gettando le fondamenta per il completo adattamento di metodi come il $P_3 - T_3$.

Il presente lavoro di tesi è stato svolto nell'ambito di una collaborazione scientifica tra il Politecnico di Torino e il Centro Italiano Ricerche Aerospaziali CIRA S.c.p.a., in sintonia con i progetti europei STRATOFLY e MORE and LESS.

Contents

List of Figures

List of Tables

Nomenclature

Symbols

$\bar{R}$	specific universal ideal gas constant [m^2 s^{-2} K^{-1}]
$\dot{m}$	mass-flow rate [kg/s]
$\mathcal{T}$	net thrust [kg m s^{-2}]
$\mathcal{T}_u$	unistalled thrust [kg m s^{-2}]
A	transversal area $[m^2]$
a	speed of sound [m/s]
c_p	heat capacity at constant pressure [m^2 s^{-2} K^{-1}]
C_x	drag coefficient
f	fuel-to-air ratio
f_{sto}	stoichiometric fuel-to-air ratio
H	heat of reaction [MJ/kg], humidity factor
h	specific entalpy [m^2 s^{-2}], relative humidity
I_{sp}	specific impulse [m s^{-1}]
m	mass [kg]
P	power [kg m^2 K^{-3}]
p	pressure [kg m^{-1} K^{-2}]
p^0	total pressure [kg $m^{-1}s^{-2}$]
q	heat [kg m^2 s^{-2}]
R	universal ideal gas constant [m^2 s^{-2} K^{-1}]
T	temperature [K], thrust [kg m s^{-2}]
t	time [s], residence time [s]
T^0	total temperature [K]
V	volume [m^3]
v	velocity [m/s]
W	fuel flow [kg/s]
z	altitude [m]

Acronyms

NO_x	nitric oxid
AR	Area Ratio
ATR	Air Turbo Rocket
ATREX	Air Turbo Ramjet with Expander Engine
BFFM2	Boeing fuel flow method 2
CFD	Computational Fluid Dynamics

CIRA	Centro Italiano Ricerche Aerospaziali
DLR	Deutsches Zentrum für Luft- und Raumfahrt
DMR	Dual Mode Ramjet
$EINO_x$	NO_xEmission Index
FAR	fuel-to-air ratio
GHG	green house gases
HEX	heat exchanger
HSI	high speed intake
ICAO	International Civil Aviation Organization
ISA	international standard atmosphere
LES	large-eddy simulation
LH_2	liquid hydrogen
LSI	low speed intake
PAH	polycyclic aromatic hydrocarbons
SABRE	Synergic Air Breathing Engine
TPR	total pressure recovery
TSTO	two stages to orbit
UVB	ultraviolet B-rays
VKI	von Kàrmàn Institute for Fluid Dynamics
M	Mach number

Greek letters

α_c	intake mass capture ratio
β	compression ratio, expansion ratio
δ	pressure loss, pressure ratio
η	adiabatic efficiency
η_m	mechanic efficiency
γ	adiabatic expansion coefficient
ϕ	equivalence ratio
ρ	density [kg m^{-3}]
ε	penumatic efficiency
ϑ	temperature ratio

Chapter 1

Introduction

1.1 Main objectives

This research aims to a deep understanding of the new type of engines that will be mounted on a new generation of hypersonic vehicles. In particular, Air Turbo Rocket (ATR) engine will be deeply analyzed, enriching and updating the existing analytical models built to compute its performances. The first part of the work will consist in the *development of an upgraded numerical model*, based on the previous model found in literature, which will represents the air turbo rocket in each flight condition.

The objective of the first part of the work is to obtain a reliable prediction of two infra-cycle thermodynamic variables: temperature and pressure at the injection in the combustion chamber, before the combustion, in order to provide numerical inputs for the calculation of Nox emission by means of 0D kinetic simulation at specific points along the stratofly trajectory to which calculate the NO_x emissions for particular points in STRATOFLY trajectory. This data will represent the base of the second part of the work.

The second part of this study will aim to considering the *environmental impact* of this propulsive technology. Basing calculation on the variables computed by the updated model, it will be possible to obtain with accuracy the emission in terms of $EINO_x$, using a chemical kinetic scheme. This emission index will be also calculated implementing the $P_3 - T_3$ emission prediction method, that will be reshaped and enriched in order to predict the emissions of combined cycle and hydrogen based engines.

1.2 State of the Art of hypersonic propulsion

In order to match higher mission profiles, different propulsive cycles have to be implemented, enhancing the performances of traditional engines. Missions for trans-atmospheric vehicle requesting high-speeds for long-range transports (such as the case

study of this thesis work), orbital space transports and military strikes put a severe demand on the propulsion system, which must deliver a high performance in a wide range of Mach numbers. Referring to the long-range transport of goods and peoples, nowadays commercial aircrafts rely in term of propulsion system on engines belonging to turbofan family, due to the fact that the thrust needs to satisfy a range of Mach from 0 to 0.9 along a trajectory from 0 to $11\,\mathrm{km}$ of altitude.

Turbofan engines, like turbojet engines, use of turbomachinery to compress the ingested air: these are in fact used to fly at relatively low speed, where a ram compression from the intake would not be enough to operate an efficient cycle. Generally speaking, the compression is hence provided by a series of axial compressors, driven by the power obtained from the expansion of the working fluid through a turbine. Indeed these two turbomachinery elements reveals the main problems:

- The compression ratio is strongly limited by aerodynamic effects, and, since the low flight speed, it's obtained just from the compressor.

- The power demanded to the turbine is limited by the temperature of the incoming fluid in terms of thermal resistance of the blades.

In order to fly over a wider range of flight speed and altitudes, unconventional engine architecture should be taken into account; a promising propulsion concept is a rocket and turbine-based combined-cycle engines constitute derivatives from the Brayton cycle which extend the use of turbomachinery in the compression system up to Mach 4. This kind of engine works as an air-breathing engine for the first part of trajectory and as a rocket when the altitude is too high and the atmosphere is not dense enough.

Perfect examples of this kind of technology can be found since the late 80's with the ATREX project, an ancestor of the modern Air-Turbo Rocket further presented, up to the present day with engine like Scimitar, SABRE and ATR. The ATREX engine is a precooled air turbo rocket developed in Japan by Prof. N. Tanatsugu in the 1980's, and it has been developed as a fly-back booster up to Mach 6 on a TSTO (Two Stages To Orbit) space plane [21]. For more modern examples it is possible to refer to the SABRE (Synergic Air-Breathing Rocket Engine); the SABRE is a precooled air breathing rocket engine, hydrogen fueled, capable to accelerate from Mach 0 at ground level to Mach 5 at 25 km of altitude. SABRE will be mounted on Skylon, a single stage to orbit spaceplane designed for transport missions from ground to orbit [9] Fig. 1.1. Another valid example of modern combined cycle engine, not precooled , is the ATR equipping the LAPCAT II MR2.4. LAPCAT is a commercial waverider transport plane, and it constitutes the projectual base of STRATOFLY MR3 as discussed in the following paragraph. The STRATOFLY project, the most modern conceptual application of combined-cycle propulsion technology, will be further described in the next section and its propulsive system constitutes the case study of this work.

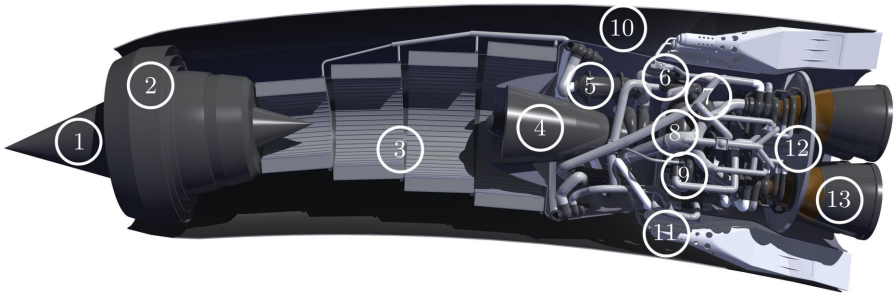

Figure 1.1. *[5] SABRE median section:* ***1*** *movable spike,* ***2*** *intake,* ***3*** *precooler,* ***4*** *air compressor,* ***5*** *pre-burner and reheater,* ***6*** *helium circulator,* ***7*** *H2 pump,* ***8*** *He turbine and regenerator,* ***9*** *LOx pump,* ***10*** *spill duct,* ***11*** *ramjet burners,* ***11*** *heat shield,* ***13*** *thrust chamber.*

1.2.1 Case study: STRATOFLY project

The STRATOFLY (*Stratospheric Flying Opportunities for High-Speed Propulsion Concepts*) project was born in the framework of Horizon 2020, a funding program created by the European Union to support and promote research, implementing also a view to innovative environmental research relative to the European policy (*European environmental research and innovation policy*), which aims to transform a European program of sustainable development and green economy into reality. In this context STRATOFLY aims to deepen the study of the potential of high-speed civil aircraft from a technical, environmental and economic point of view. In particular, STRATOFLY has its roots in previous projects, which constitute the previous state of the art of the research in this field and whose prototypes will be cited as a design basis from different points of view: starting from refining the LAPCAT II - MR2.4 waverider concept, all the aspects of its design have been refined. This allowed, in a highly multidisciplinary research environment, to face technological criticalities with expedients that would allow the feasibility of a hypersonic commercial flight [20].

The actual state of the art is represented by STRATOFLY MR3 indeed, developed thanks to the collaboration of some of the best universities and research centers in Europe, all coordinated by Politecnico di Torino (coordinator of the project and deputed to the system design, the life cycle cost estimation and the safety assessment). The designed MR3 vehicle shall be able to satisfy the following high-level requirements, bringing an absolute innovation to the sector [6]:

- Shorten the flight time of one order of magnitude with reference to conventional long-haul flights.
- Transport 300 passengers as reference payload.
- Flight along long-haul and antipodal routes up to 19000 km Fig. 1.2.
- Reach Mach 8 in cruise.

- Fly in the stratosphere between 30 and 36 km in cruise

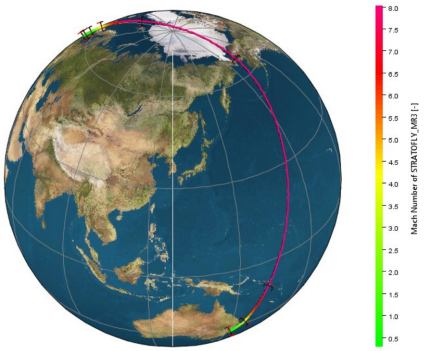

Figure 1.2. *Overview of complete trajectory BRU-SYD.Trajectory is characterized by Mach number on the right.*

STRATOFLY MR3 maintains the waverider configuration of MR2.4, with the whole propulsive plant dorsal-mounted (over the passenger cabin), basing the air ingestion on an air intake embedded intro the airframe, Fig. 1.3. The integration allows a body shape that increases the aerodynamic efficiency while optimizes the internal volume.

Figure 1.3. *Perspective of the STRATOFLY MR3 hypersonic cruiser.*

STRATOFLY propulsion plant

The propulsion plant of STRATOFLY MR3 is based on the original propulsion architecture from LAPCAT MR2.4: the whole layout features a flow path mounted over the passenger cabin, that is the result of the integration of two different propulsive technologies, six air turbo-rocket (ATR) further described and a dual mode ramjet (DMR). ATR is a rocket based air-breathing engine, while the DMR is an air-breathing engine that can work in a ramjet (subsonic combustion) or in a scramjet (supersonic combustion) configuration. The two engines are essentially separated in terms of internal fuel and air flow path, but they share a common variable geometry intake which, based on the flight condition, will redirect the needed air mass flow to the ATR or to the DMR ducts [15],

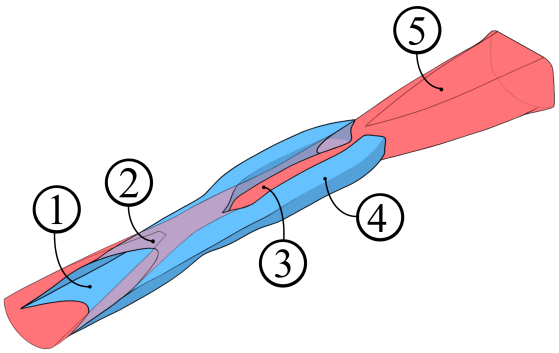

Figure 1.4. *STRATOFLY MR3 internal flow paths:* ***1*** *Low Speed Intake,* ***2*** *High Speed Intake,* ***3*** *DMR duct,* ***4*** *ATR duct,* ***5*** *common nozzle.*

Fig. 1.4. The ATR, as it will be further described in Chap. 1.3, will operate alone in the range from Mach 0 to Mach 4, while will be progressively shut down in until Mach 4.5 is reached, when the whole thrust will be provided by the DMR; ranging from 0 to Mach 4.5, the intake will regulate and eventually redirect the ingested airflow, in order to satisfy the working conditions of each engine. The regulation, relegated to the intake (the same present in LAPCAT MR2.4), is done through a series of compression ramps which create a three-dimensional complicate shock pattern. Both air turbo-rockets and duel mode ramjet share a common nozzle, assumed to be a duel-expander type: the inner section is constituted by the nozzle of the dual-mode ramjet, while the outer contour comprises the divergent section of the air turbo-rocket nozzles. Both nozzles can vary their throat area in order to adapt the expansion ratio. The flow field inside the nozzle is a complex fluidodynamic configuration, which varies depending on the working regime: ATR alone, combination of ATR and DMR and DMR alone

1.3 Air-Turbo Rocket engine

1.3.1 ATR characteristics

The air turbo-rocket combines elements from turbojet, ramjet and rocket motors, and makes use of a different propellant: liquid hydrogen, which problems and benefits will be further described in Sec. 3.1. The unique architecture provides unique performances indeed, keeping together the advantages of air breathing and rocket engines: ATR provides an higher specific impulse compared to a rocket engine, and a higher thrust-to-weight ratio, constituting an excellent engine choice for a large range of speed and altitudes. For these characteristics, ATR is an excellent accelerator engine, providing high thrust level allowing to push the vehicle far over transonic and drag rise speeds, reaching low hypersonic speed regime. Despite being an airbreathing engine, the specific impulse I_{sp}, as found inside the solution space computed by [5] and performances data provided by VKI discussed in Sec.2.5, is not strongly variable along flight speed: unlike ATR, the

sensitivity of the specific impulse of a turbojet to changes in therm of throttle, brings large changes in fuel consumption rate. Because of these unusual characteristics, ATR can perform well in a wide range of situation, and for these reasons it would be an ideal choice to cover Stratofly mission from takeoff to Mach 4.5 acceleration. On the other hand, ATR suffers of problems coming from turbomachinery characteristics and couplings; as exposed by [2] in a conventional airbreathing turbomachinery-based engine, the turbine power output is coupled to the compressor performances: if the compressor enters in a critical working regime, such as a stall or a surge, the turbine output changes directly under the influence of the airflow coming coming from the compressor, and the whole system reacts moving the working point to off-design conditions, preventing itself from damages. This situation, because of its system design, does not arise in ATR, where the power delivered to the turbine is independent of fan performances.

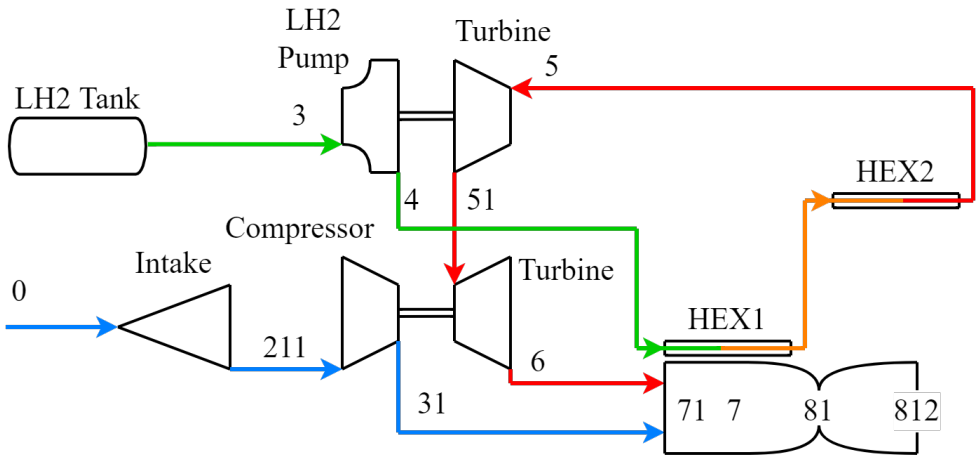

Figure 1.5. *Air Turbo-Rocket cycle.*

1.3.2 Engine architecture

The engine cycle realized by the ATR mounted in STRATOFLY MR3 is reported in Fig. 1.5, and the turbomachinery plays a relevant role, allowing during the early ascent to produce static thrust and at low Mach numbers. As it would be exposed further considering the behaviour of the fan pressure ratio β_f, for growing Mach the compression from the fan will be gradually replaced by ram compression from the intake, allowing the engine to work as a ramjet.

Following the air flow from the free stream [*0*], it passes first through the intake, which gives (if the flight speed is relevant) an initial compression. After the ram compression [*211*], the flow is pressurized by the fan [*31*] and sent to the combustion chamber [*71*]. The fan is driven by a turbine [*6*] which drags the fuel pump too [*4*], and which is powered by the regeneratively heated fuel, passing through two heat exchangers [*5*].

Describing the fuel cycle, liquid Hydrogen is stored at a pressure of $3\,\mathrm{bar}$, a temperature of $20\,\mathrm{K}$ and a density of $71\,\mathrm{kg/m^3}$ [5], and it is pressurized with a turbo-pump. The regenerative heat exchangers are built along the combustion chamber and the nozzle, cooling these lasts while energizing the fuel, which changes from liquid to gaseous phase and expand through the turbine. After this first expansion, Hydrogen is injected in the combustion chamber [*71*] and burns with the air [*7*]. Burning gases are discharged through a converging-diverging nozzle.

Chapter 2

Numerical Modeling

In this chapter it is presented a state of art of the mathematical models of the ATR, developed [16] in various degree of deepness. The preliminary step was the completely and detailed modeling of the ATR engine in order to create a more complete propulsive database. The development of this model starts from the revisioning of the pre-existing models, that will be described with more details in the next sections. The work is conducted through a step by step process, focusing on different section of the cycle and analyzing the impact of each improvement and correction on infra cycle variables, and comparing the results with the available propulsive database. The approach to the testing of each improvement is variable depending on the part of the cycle that has to be optimised, and it will be deeply explained in the further sections.

2.1 MatLab®

The following analysis are all developed on the MatLab System, a C-based programming platform which integrates computation, visualization and programming in an user-friendly environment. It has been developed by MathWorks®, which is the supplier of the programming environment. The MatLab System consists of three main parts:

1. **MatLab language**
   The language is an high-level matrix and array language that implements control flow statements, functions and data structures. Any basic elements does not requires dimensioning: this feature simplify the programming a lot, avoiding many practical problem during the computing and the variables declaring due to previous memory allocation.

2. **MatLab graphic handling**
   The MatLab environment includes high-level commands and tools for data visualization. It allows the visualization, image processing and also animation of 2D and 3D data. Any appearance is deeply customizable both through programming

and through MatLab Graphic User Interface.

3. **MatLab function library**
   The whole system is based on a vast library of algorithms and functions, which allows any mathematical operation. The function integration is easy-to-use and the community can develop complex and dedicate functions to share with other users. Complex solutions dedicated to specific applications are organized in specific tools that are downloadable directly from the MatWorks platform: the toolboxes extend the MatLab environment to particular classes of problems, such as for example curve fitting, flight dynamic modeling, meteo calculations.

2.2 Atmosphere model

The modeling of variable flight conditions in term of flight quote, from 0 to 26 km of altitude along STRATOFLY trajectory, requires an atmosphere model in order to define the environmental conditions: temperature, pressure and density. These variables are computed through the following model, taken from [22] and based on International Standard Atmosphere (ISA).

STANDARD CONDITIONS			
Temperature	$\mathbf{T}_{st}$	[K]	288.15
Pressure	$\mathbf{p}_{st}$	[Pa]	101325
Density	ρ_{st}	[Kg/m^3]	1.225

Table 2.1. *Initial condition of the atmosphere model, referred to the standard conditions.*

- $\mathbf{0 < z < 11000\ m}$

$$T_0 = T_{st} - 0.0065z \tag{2.1}$$

$$p_0 = p_{st}\left(1 - 0.0065\frac{z}{T_{st}}\right)^{5.2561} \tag{2.2}$$

$$\rho_0 = \rho_{st}\left(1 - 0.0065\frac{z}{T_{st}}\right)^{4.2561} \tag{2.3}$$

The conditions at $z_s = 11\,\mathrm{km}$ are reported in the Tab. 2.2:

CONDITIONS AT $z = 11\,000\,\mathrm{m}$			
Temperature	$\mathbf{T_{11}}$	[K]	216.65
Pressure	$\mathbf{p_{11}}$	[Pa]	22630
Density	$\rho_{\mathbf{11}}$	[Kg/m^3]	0.364

Table 2.2. *Conditions at the beginning of the Stratosphere.*

- $\mathbf{11000 < z < 20000\ m}$

$$T_0 = T_{11} \tag{2.4}$$

$$p_0 = p_{11} \exp\left[\frac{-g(z - z_{11})}{RT_{11}}\right] \tag{2.5}$$

$$\rho_0 = \rho_{11} \exp\left[\frac{-g(z - z_{11})}{RT_{11}}\right] \tag{2.6}$$

CONDITIONS AT $z = 20\,000\,\mathrm{m}$			
Temperature	$\mathbf{T_{20}}$	[K]	216.65
Pressure	$\mathbf{p_{20}}$	[Pa]	5471.65
Density	$\rho_{\mathbf{20}}$	[Kg/m^3]	0.089

Table 2.3. *Conditions at* $z = 20\,000\,\mathrm{km}$.

- $\mathbf{z > 20000\ m}$

$$T_0 = T_{20} + 0.001(z - z_{20}) \tag{2.7}$$

$$p_0 = p_{20}\left(1 + 0.001\frac{z - z_{20}}{T_{20}}\right)^{\frac{-g}{0.001 \cdot R}} \tag{2.8}$$

$$\rho_0 = \rho_{20}\left(1 + 0.001\frac{z - z_{20}}{T_{20}}\right)^{\frac{-g}{0.001 \cdot R}-1} \tag{2.9}$$

The atmosphere model allows to calculate the speed of sound a, an essential variable that will be used to compute the flight speed:

$$a_0 = \sqrt{\gamma \overline{R} T_0} \tag{2.10}$$

where γ is the adiabatic expansion coefficient of the air (equal to 1.4) and $\overline{R}$ is the specific universal gas constant (with a value of $287.05\,[\mathrm{J}/(\mathrm{kgK})]$). In Fig. 2.1 are reported temperature, pressure and density along with the altitude; different gray scale

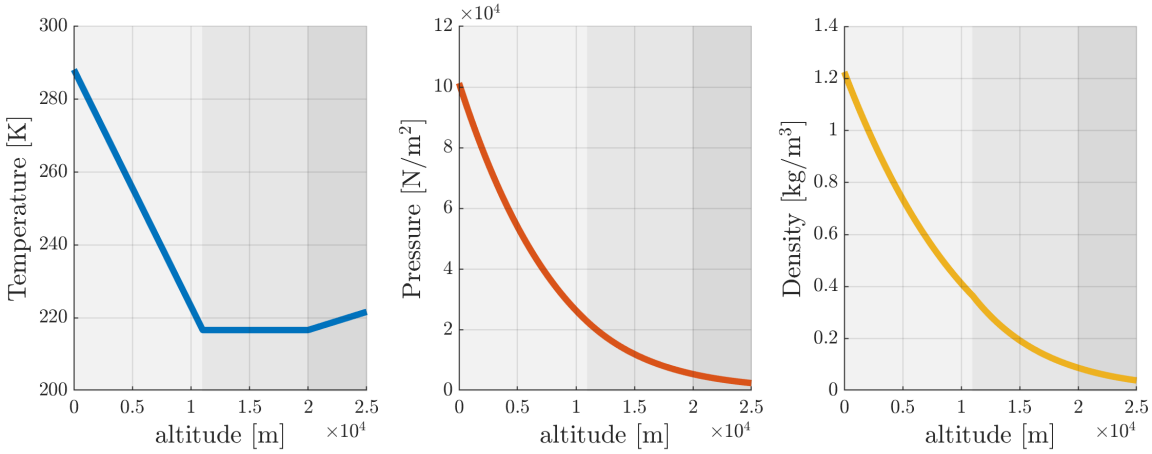

Figure 2.1. *Thermodynamic coordinates of the atmosphere model in a range of altitude from 0 to 25 km, representative of STRATOFLY trajectory.*

marks the different approximation used to compute the atmospheric variables related to the altitude.

2.3 Previous engine model

The first purpose of this thesis work consists in analyzing, as deep as possible, the available models of the engine to build a consistent input for the predictive method exposed in Sec. 3.6. The available models have been developed in [16], in which various assumptions of increasing complexity summarize the behavior of ATR in its flight regimes. The most advanced of the proposed models relies on the two different sides of ATR working principles: subsonic regimes are well represented by a turbojet with afterburner, while for Mach greater than 2.5, a ramjet with compressor model is used.

2.3.1 The model of main component

The following description gives an overview of the equations that constitute each component of the most complete model present in literature, including the calculations regarding the atmosphere characteristics along STRATOFLY trajectory. According to Fig. 1.5, the equations presented in this section models both the airflow path and the fuel cycle. All the input used are summarized in the next paragraph and presented in the Tab. 2.3.2. A block scheme representing the model is also presented in Fig. 2.2.

$\underline{\mathbf{0 \rightarrow 211}}$ INTAKE

The intake provides to the regulation of the incoming air mass-flow and to the ram compression of the fluid (especially at high Mach numbers). The diffuser is assumed to

be adiabatic and the intake pneumatic efficiency ε_d is assumed to be constant.

$$\begin{aligned} T_{211}^0 &= T_0^0 \\ p_{211}^0 &= \varepsilon_d p_0^0 \\ \dot{m}_0 &= \rho_0 A_0 u \end{aligned} \tag{2.11}$$

Referring to Eqz. 2.10 the flight speed u is given by the following equation:

$$u = M a_0 \tag{2.12}$$

211 → 31 FAN

A fan provides additional flow compression when Mach is not high enough for ATR to work in full ramjet configuration. Compressor pressure ratio β_f is assumed to be constant and equal to 8.0.

$$\begin{aligned} T_{31}^0 &= T_{211}^0 \left[1 + \frac{1}{\eta_c} \left(\beta_f^{\frac{\gamma-1}{\gamma}} - 1 \right) \right] \\ p_{31}^0 &= \beta_f \, p_{211}^0 \end{aligned} \tag{2.13}$$

3 → 4 FUEL PUMP

The fuel pump is the first component of the fuel cycle and it is treated as a compressor stage that, through a compression ratio β_p, elevates the pressure of the fuel in order to feed the turbine. No LH_2 changes in phase are considered indeed, the fuel remains in liquid state through the whole compression process.
Determined the adiabatic pump efficiency η_p, propellant adiabatic expansion coefficient and specific heat γ_{Lh} and $c_{p.LH}$, fuel pressure and temperature can be found.

$$\begin{aligned} T_4^0 &= T_3^0 \left[1 + \frac{1}{\eta_p} \left(\beta_p^{\frac{\gamma_{LH}-1}{\gamma_{LH}}} - 1 \right) \right] \\ p_4^0 &= \beta_p p_3^0 \end{aligned} \tag{2.14}$$

4 → 6 TURBINE

The turbine drives both pump and fan, and allows the gas to expand until it reaches the pressure of the airflow p_{31}^0, favouring the mixing in the combustion chamber. Determined the pressure that has to be reached, the turbine expansion ratio β_t is computed, and so the exit fuel temperature.

$$\begin{aligned} \beta_t &= \frac{p_4^0}{p_{31}^0} \\ p_6^0 &= \frac{p_4^0}{\beta_t} \\ T_6^0 &= T_4^0 - \frac{c_p}{c_p'} \frac{1}{\eta_t} \frac{T_4^0 - T_3^0}{1 + f_{\text{sto}}} \end{aligned} \tag{2.15}$$

6 & 31 → 71 MIXER

A virtual mixer is located before the combustion chamber. The total pressure of incoming fuel and air flows is imposed to be the same, and the temperature after the mixing is calculated imposing the thermodynamical equilibrium considering an isothermal process:

$$T_{71}^0 = \frac{c_p T_{31}^0 + f_{\text{sto}} c_{p,LH} T_6^0}{c_p'(1+f)} \tag{2.16}$$

71 → 81 COMBUSTION CHAMBER

Combustion process is modeled it were a heating process, allowing to write a total enthalpy equilibrium to find the temperature reached after the combustion. The fuel-to-air ratio is treated as a constant for each flight condition and equal to its stoichiometric value: $f_{\text{sto}} = 0.029$. From enthalpy balance, knowing adiabatic combustor efficiency η_b, combusted gases specific heat c_p' and heat of reaction of LH2, it's possible to obtain the temperature after the combustion.
Knowing the combustor pneumatic efficiency ε_b, the pressure after combustion is obtained.

$$\begin{aligned} T_{81}^0 &= T_{71}^0 + \eta_b f_{\text{sto}} \left(\frac{H_i}{c_p'} \right) \\ p_{81}^0 &= \varepsilon_b \, p_6^0 \end{aligned} \tag{2.17}$$

After the combustion, the combusted gases undergo a different process depending on the flight regime, as anticipated earlier in the introduction of this section. If the speed of the aircraft is lower than Mach 2.5, the engine is modeled through a turbojet with afterburner, else if the speed is greater of Mach 2.5 (up to Mach 4) ATR is represented by a ramjet with a compressor.
In the *first case* (Mach lower than 2.5), based the calculations on a turbojet model, the flow after the combustion is virtually expanded through another turbine posed between the combustion chamber and the exhaust nozzle. Furthermore in this situation the fuel cycle is neglected because the turbine power is computed just by considering the power delivered to the compressor, and the propellant is supposed to be injected without the work of a dedicated pump.

81 → 811 TURBINE *(turbojet model)*

The turbine expansion ratio β_t is calculated from balance equation at the shaft between turbine and fan, knowing compressor and turbine mechanic efficiencies:

$$\begin{aligned}
\beta_t &= \left[\frac{1 - c_p(T^0_{31} - T^0_{211})}{c'_p \eta_{mc} \eta_{mt} \eta_t (1+f) T^0_{81}}\right]^{\frac{-\gamma'}{\gamma'-1}} \\
T^0_{811} &= T^0_{81} - \frac{c_p}{c'_p} \frac{1}{\eta_{mc}\eta - mt} \frac{T^0_{31} - T^0_{211}}{1+f} \\
p^0_{811} &= \frac{p^0_{81}}{\beta_t}
\end{aligned} \tag{2.18}$$

In the *second case* (Mach greater than 2.5), the model relies on the scramjet with compressor adaptation: after the combustion the flow expands directly into the nozzle.

81 → 812 NOZZLE

The whole cycle ends with the expansion through a nozzle, that is considered always adapted. Following this approximation, data about nozzle geometry can be cut off, and exit total pressure and temperature are calculated knowing the pneumatic nozzle efficiency ε_n and supposing this last adiabatic.

$$\begin{aligned}
T^0_{812} &= T^0_{81} \\
p^0_{812} &= \varepsilon_n \, p^0_{81}
\end{aligned} \tag{2.19}$$

Finally, exit flow speed w_e, required to calculate the thrust, is computed by the equivalence of total enthalpy.

$$w_e = \sqrt{2 c'_p T^0_{812} \left[1 - \left(\frac{p_0}{p^0_{812}}\right)^{\frac{\gamma'-1}{\gamma'}}\right]} \tag{2.20}$$

Knowing the speed of the flow exiting the nozzle, the gross thrust is computed as shown in (2.21):

$$\mathcal{T}_{\text{ATR's}} = \dot{m}_0[(1+f)w_e - u] + A_e(p_e - p_0) \tag{2.21}$$

2.3.2 Model input data

In Tab. 2.3.2 are presented the input data, found in literature, utilised in [16] for the ATR Complete Model.

Engine Data			
Overall Pressure Ratio - Fan	β_f	[-]	8.0
Overall Pressure Ratio - Pump	β_p	[-]	15.0
Pneumatic Efficiency - Intake	ε_d	[-]	0.98
Pneumatic Efficiency - Combustor	ε_b	[-]	0.95
Pneumatic Efficiency - Nozzle	ε_n	[-]	0.98
Adiabatic Efficiency - Fan	η_f	[-]	0.88
Adiabatic Efficiency - Combustor	η_b	[-]	0.90
Adiabatic Efficiency - Turbine	η_t	[-]	0.80
Mechanic Efficiency - Fan	η_{mf}	[-]	1.00
Mechanic Efficiency - Turbine	η_{mt}	[-]	0.95
Propellant Data			
Propellant storage temperature	T_3	[K]	20
Propellant storage pressure	p_3	[bar]	3
LH2 heat of reaction	H_i	[MJ/kg]	120.9
LH2 adiabatic expansion coefficient	γ_{LH}	[-]	1.5
LH2 specific heat	$c_{p,LH}$	[J/(kgK)]	14435
Stoichiometric fuel ratio	f_{sto}	[-]	0.029
Combusted adiabatic expansion coefficient	γ'	[-]	1.33
Combusted specific heat	c'_p	[J/(kgK)]	1900
Geometrcal Data			
Inlet Area	A_0	[m^2]	37.7
Outlet Area	A_{812}	[m^2]	20.6

Table 2.4. *Input data for Complete Model.*

2.3.3 Model flowchart

In Fig. 2.2 is presented a flowchart of the complete model. It initially shows separately the air and the fuel path, that will mix in the mixer before the combustion. After the combustion, the decision block separates the turbojet approximation (right path) and the ramjet approximation (left path) depending on the flight Mach. Eventually after the turbine expansion in the turbojet path, the burned flow expands in the nozzle: the

performances are carried out through the calculation presented in the next paragraph and stored as outputs. Black modules instead represents the inputs in term of propellant data and engine parameters (both shown in Tab. 2.3.2), and the inputs from the analyzed flight conditions in term of Mach and altitude.

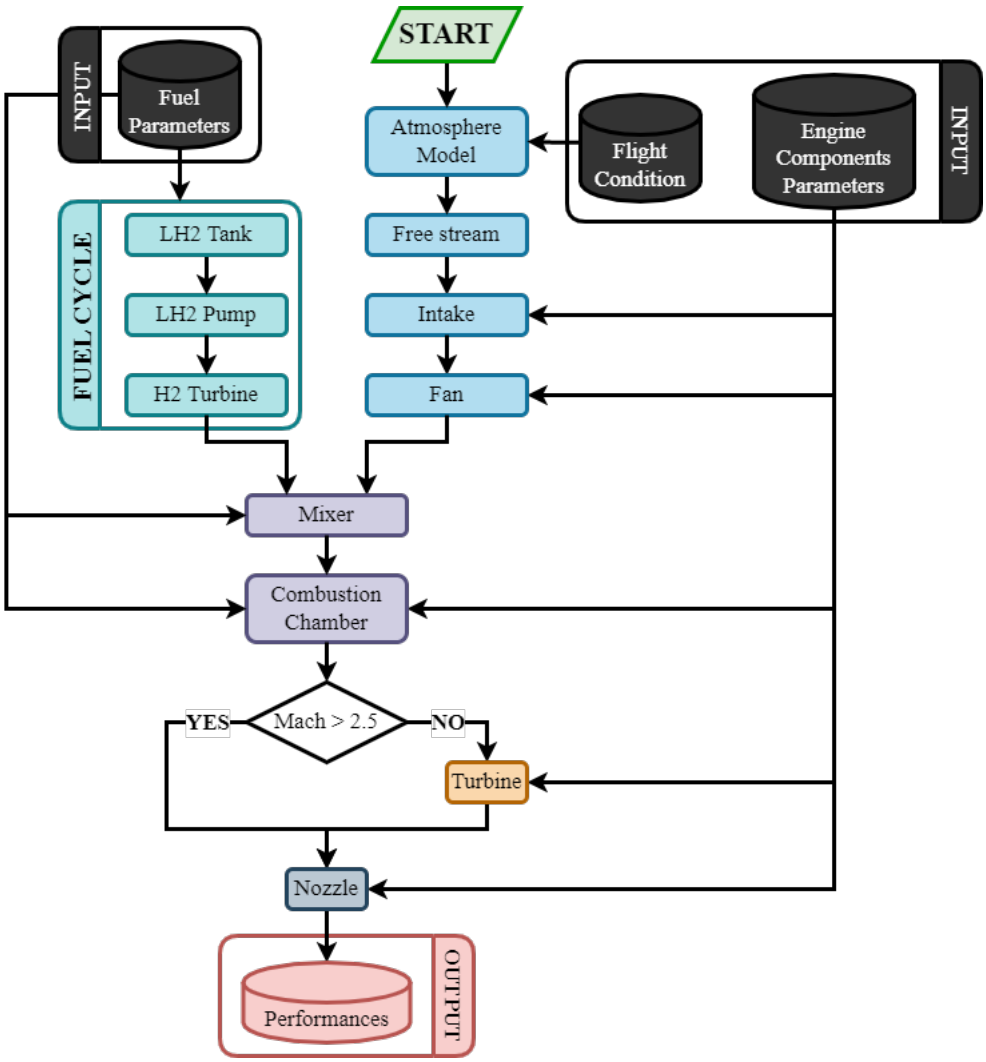

Figure 2.2. *ATR Complete Model: flowchart.*

2.3.4 Model output

A summary of results in terms of thrust and errors relative to the dataset are reported in the following tables 2.3 and graphs. The validation has been done relatively to a dataset providing the performances of LAPCAT MR2 (as reported in the caption in Fig. 2.3), that is accelerated via the same ATR of STRATOFLY.

The entity of the error has been evaluated through the Eq. (3.40):

$$\text{Err } [\%] = \frac{T_{\text{ref}} - T_{\text{model}}}{T_{\text{ref}}} \times 100 \tag{2.22}$$

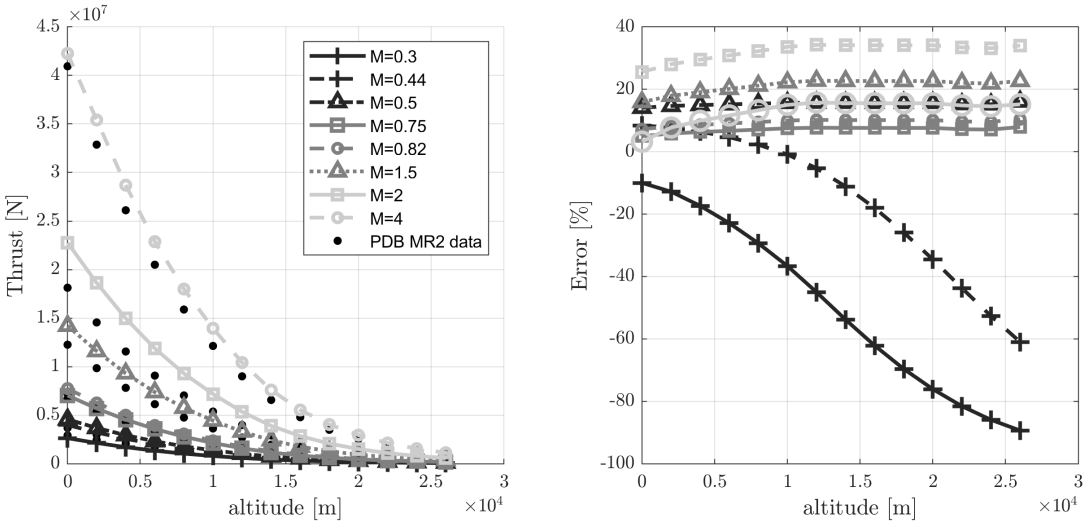

Figure 2.3. *Output and errors of the ATR modeled as a ramjet+compressor.*

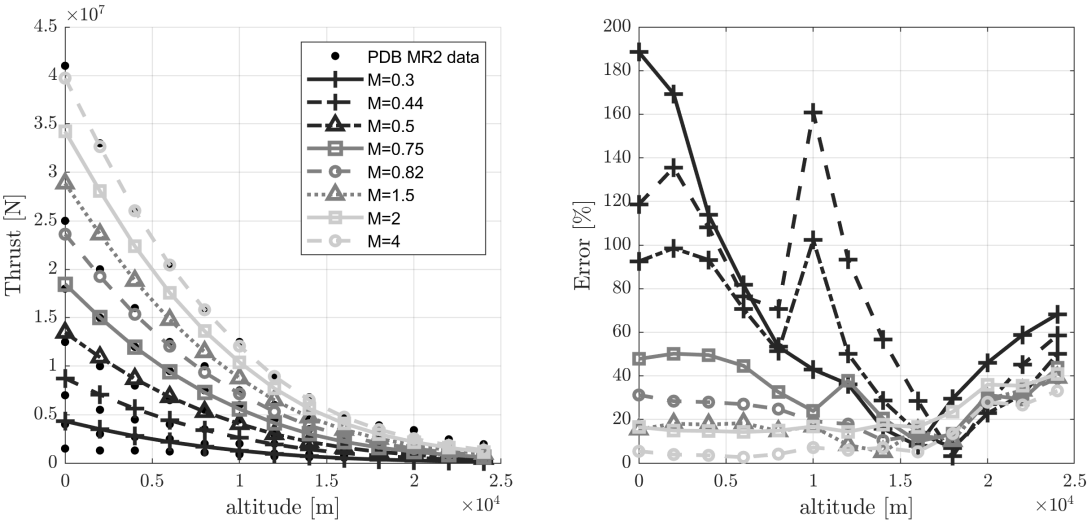

Figure 2.4. *Output and errors of the ATR modeled in the complete model, as a turbojet for subsonic and low-supersonic and a ramjet for high supersonic speed.*

where T_{ref} stands for the reference data and T_{model} represents the computed data from the model.

As it possible to observe in Fig. 2.4, the previous model over-extimates the performances at low Mach numbers. This could be justified due to a strong input approximation over the fan pressure ratio, fixed at a constant value. The β_f is crucial in the subsonic, a regime in which the ram compression is not strong, and the majority of the compression work is deputed to the fan. The error also arises with altitude; the cause could be attributed again to the fan pressure ratio, that is constant also during a phase of the trajectory in which the ram compression prevails. Probably, in the interval from 1.5 to 1.8 km in which each Mach number shares a low error, the combination of ram compression ad fan compression matches the reference value.

2.4 Updates to the previous model

The following improvements analysis is conducted via a multi parameter optimisation, targeting an optimal solution space for each component. Relying on these results, a stronger feedback in term of infra cycle data and turbomachines performances is available. The validation of the updates and the influence on the computing of propulsive performances are exposed in the dedicated paragraph in Chap. 4.

2.4.1 Subsystems

Intake

The ATR operates alone in the range from Mach 0 to Mach 4, and it will be progressively shut down until Mach 4.5 is reached, when the total amount of necessary thrust will be provided by the DMR; ranging from 0 to Mach 4.5, the intake will provide to the ingestion of the correct airflow in order to satisfy the working conditions of each engine. The whole regulation is relegated to the intake itself, which behavior is summarized considering that the inlet splits the airflow in two different paths; hence two equivalent distinct intakes are considered together with their respective performances in terms of air capture and total pressure recovery: the low speed intake (LSI, deputed to feed the ATR) and the high speed intake (HSI, deputed to feed the DMR). The differences in terms of the quantity of the captured air mass flow are expressed by the mass capture ratios of the low and high speed intake:

$$\alpha_c^{\text{LSI}} = \dot{m}_{\text{ATR}}/\dot{m}_0 \qquad \alpha_c^{\text{HSI}} = \dot{m}_{\text{DMR}}/\dot{m}_0 \tag{2.23}$$

where $\dot{m}_0$ is the whole captured mass flow.

In Tab. 2.4.1 are reported some values for the mass flow rates at representative Mach numbers.

	LSI		HSI	
Mach$_\infty$	**TPR** [%]	$\alpha_{\mathbf{c}}^{\text{LSI}}$ [%]	**TPR** [%]	$\alpha_{\mathbf{c}}^{\text{HSI}}$ [%]
1.5	95	51	97	15
2.0	80	55	85	18
3.0	70	52	89	37
4.0	70	52	76	41
4.5	70	51	68	44

Table 2.5. *Total pressure recovery (TPR) and capture rates (α_c) of the low speed intake (HSI) and high speed intake (HSI).*

Referring to the previous modelling of the intake, developed under the equations

Eq. (2.11), the area of the intake (the input named A_0 in Tab. 2.3.2, the same in each flight condition) is kept constant, and the variation of the captured air mass-flow rate is deputed only to the changes in density and flight speed. Based the analysis on [15] is possible to insert the term α_c, as expressed in Eq. (2.23), directly in the air mass-flow rate equation:

$$\dot{m}_0 = \rho_0 u A_0 \alpha_{c,\text{LSI}} \tag{2.24}$$

Being the mass flow rate an extensive magnitude, in order to consider the thrust of a single ATR engine, the total amount of air flow defined by (2.23) is divided by six (the number of ATR engines in the Stratofly MR3).

Another input imposed in the pre-existing model still resides in the intake, and it is particularly weighty, especially at high Mach numbers, as the errors analyzed in [16] reveals: a constant total pressure recovery (TPR) does not represent well a complex variable geometry intake which will work from Mach 0 to Mach 4.5 [15], so from a condition without ram compression to a condition where the engine works thanks only to the ram compression. Considering the TPR $\equiv \varepsilon_d$ of the intake as follow in Eq. (2.25), referring to the stations inf Fig. 1.5,

$$\varepsilon_d = \frac{p_{211}^0}{p_0^0} \ . \tag{2.25}$$

From [15] and [5] it is possible to extrapolate the behaviour of the intake's TPR through a wide range of Mach numbers: the data are particularly suitable for a modified-Akima spline interpolation, obtaining third-grade interpolations subdivided on the basis of the reference Mach intervals reported in Tab. 2.6. The choice of the interpolation method fell on the Akima spline [1] because the second grade derivative varies a lot in the extremes of the interval: for subsonic Mach numbers ε_d is equal to 1 and rapidly changes in slope growing the speed, while for growing Mach the slope decrease rapidly and $\varepsilon_d = 0.7$.

ε_d VALUES					
Mach	1.5	2.0	3.0	4.0	4.5
$\varepsilon_\mathbf{d}$	0.95	0.80	0.70	0.70	0.70

Table 2.6. *Known values of ε_d at supersonic Mach numbers.*

For the generic i-esim interval $M_0(i) \div M_o(i+1)$, the approximation is structured as follows:

$$\varepsilon_d(M_0) = a(M_0 - M_0(i))^3 + a(M_0 - M_0(i))^2 + a(M_0 - M_0(i)) + d \tag{2.26}$$

where a, b, c and d are the polynomial Akima-coefficients of the interval.
In Tab. 2.7 are reported the coefficients for the first interval, from $M_0 = 1.5$ to $M_0 = 2.0$:

$M_0 = 1.5 \div 2.0$: ε_d Coefficients			
a	**b**	**c**	**d**
0.3200	-0.3600	0.0000	1.0000

Table 2.7. *Coefficients of $\varepsilon_d(M_0)$ cubic spline approximation.*

In Fig. 2.5 is reported the behaviour of the total pressure recovery approximation (in solid line), related to the point used in the interpolation, represented by the crosses. A linear interpolation of each interval seems to bee profitable, but it would result in the loss of some information, and the application would not be easier than the Akima interpolation in term of coding.

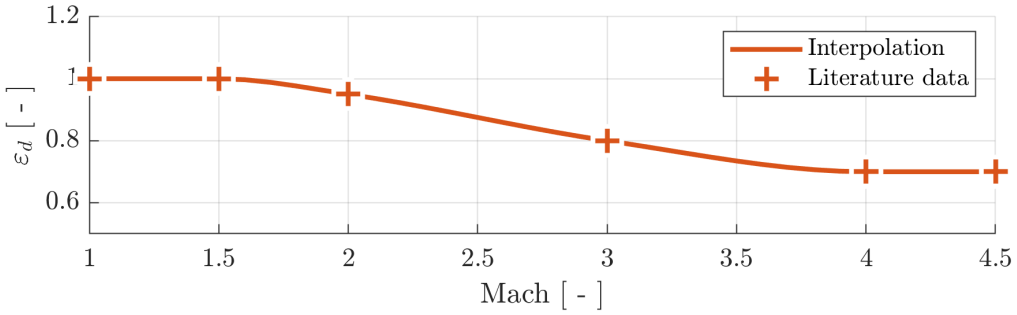

Figure 2.5. *ε_d trend as a function of Mach*

Fan stage

Along with the considerations about the intake, it follows that the fan pressure ratio could not be treated as a fixed value: for a growing Mach number, an increasing compression is demanded to the intake, and the compression deriving from to the work of fan is progressively lowered. For this reason, considering a constant fan pressure ratio is an approximation that should be refined. Due to the fact that ATR is not an existing engine with a defined turbomachine technology and geometry, it is not possible, at this level of modeling, to define an actual working map of the component. However, a better approximation could still rely on the work done by V.V.Fernandez in [5], where the optimal fan pressure ratio is deduced for each Mach and altitude. With this base is possible to carry out an interpolation that should represent in a better way the pressure jump through the compressor. The fan pressure, i.e. β_f, is defined as:

$$\beta_f = \frac{p^0_{31}}{p^0_{211}} \tag{2.27}$$

Based the interpolation on a four coefficients polynomial, the law reported in Eq. (2.28)

β_f VALUES							
Mach	0.01	0.50	0.75	1.2	2.0	3.0	4.0
$\beta_\mathbf{f}$	2.0	2.4	2.9	3.0	2.2	1.3	1.0

Table 2.8. *Known values of β_f at flight Mach numbers.*

is obtained. Though, it must be said that the following β_f interpolation is not too useful pretending to develop a working model which summarise the behaviour of the ATR in many different flight regime, but should be a better and easy-to-use base rather than considering it constant.

$$\beta_f(M_0) = p_{1f}M_0^3 + p_{2f}M_0^2 + p_{3f}M_0 + p_{4f} \tag{2.28}$$

β_f COEFFICIENTS			
$\mathbf{p_{1f}}$	$\mathbf{p_{2f}}$	$\mathbf{p_{3f}}$	$\mathbf{p_{4f}}$
0.1884	-1.34	2.119	1.901

Table 2.9. *Coefficients of $\beta_f(M_0)$ polynomial approximation.*

This first and simpler approximation of β_f, only variable with Mach number and constant along the altitude, has been refined imposing as input a certain pressure in the combustion chamber for each flight condition; the propulsive database reported temperature and pressure for the air and fuel streams entering in the combustion chamber: a more accurate value for β_f is computed retrofitting the air cycle, imposing the requested pressure as an input.

In Fig. 2.7 on the next page is possible to value the mismatch between the attended value from the database and the one computed by the model of the pressure of the air stream entering in the combustion chamber, before the retrofitting.

Observing the trend of the pressure in station [*71*], in particular at low Mach numbers (regimes in which the engine is more sensitive to the fan pressure ratio) is necessary a different β_f formulation, variable with altitude. In Fig. 2.8 on page 40 is reported the variation of β_f with altitude in subsonic flight conditions, where the mismatch with the propulsive database was higher.

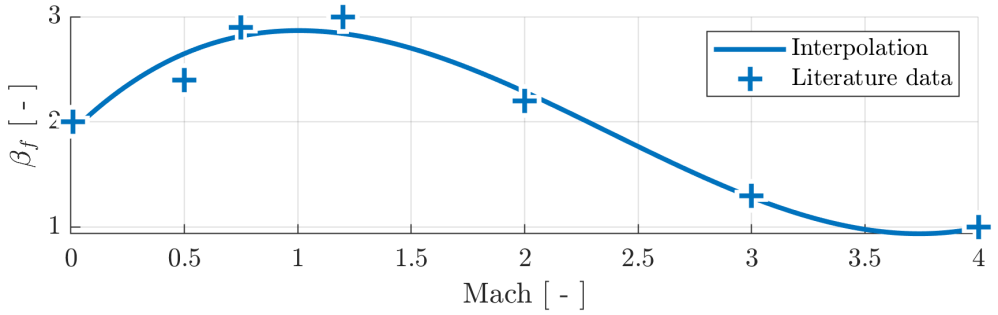

Figure 2.6. *β_f trend as a function of Mach*

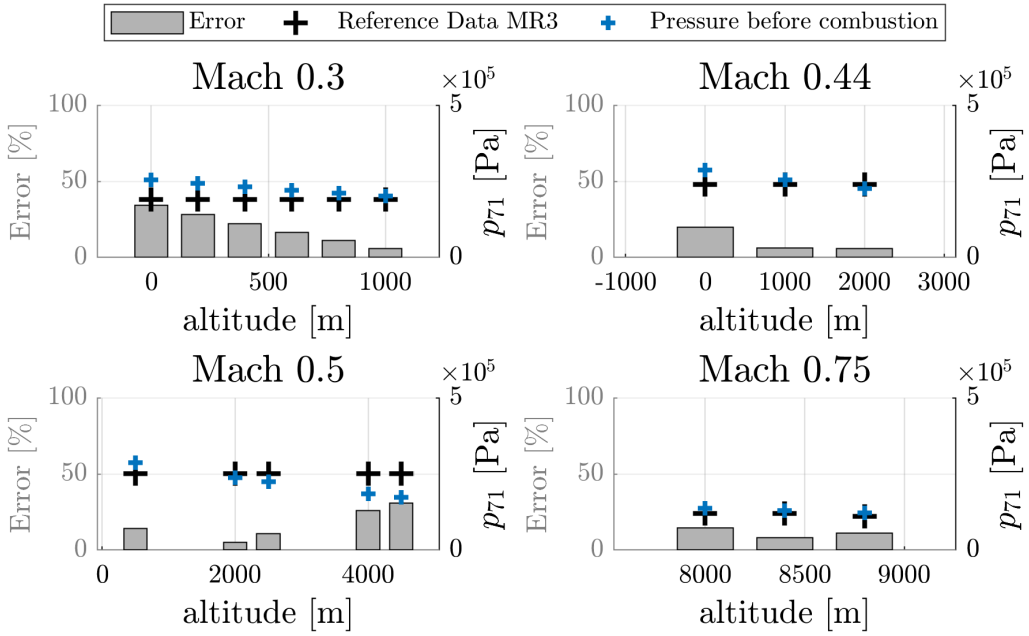

Figure 2.7. *Errors on the calculation of the pressure before combustion p_{71}, subsonic Mach.*

Fuel cycle

The fuel cycle has been reshaped thanks to data found in literature, and the performances of various component have been adapted to various working regimes. Fuel cycle is made up by essentially three main working-components: the fuel pump, the turbine and the regenerative heat exchangers; the two turbomachines performances are summarized by their efficiencies and their relative pressure ratios, while the heat exchangers influence is represented by the total amount of heat extracted from the combustion chamber and the nozzle.

Simplifying the formulation, the hydrogen is considered, when subcooled, an incompressible liquid with consant specific heat capacity, while it changes in state after the transition in the heat exchangers. The hydrogen entering the turbine is in gaseous state and it's specific heat capacity is variable with temperature. In the precedent model, the pressure ratios of the turbomachinery where considered constant, while in literature is

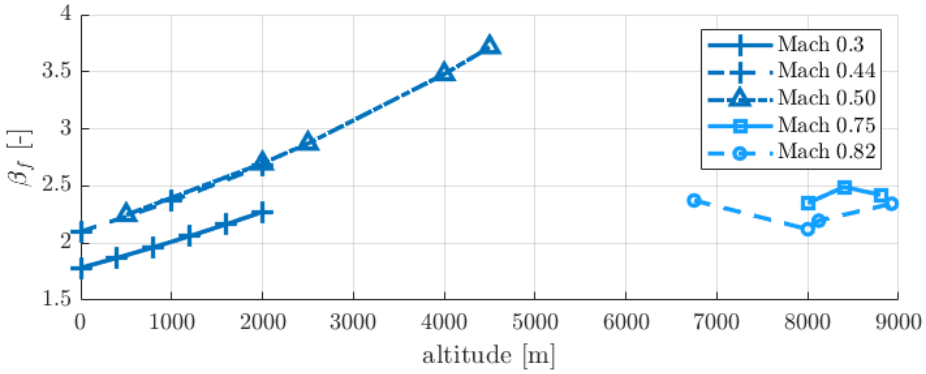

Figure 2.8. *β_f (new) trend as a function of Mach and altitude.*

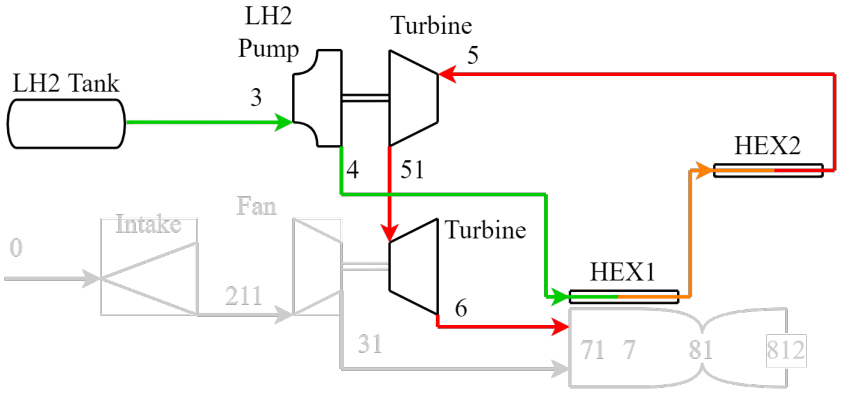

Figure 2.9. *Fuel flowpath.*

possible to find a series of values for various working regimes (defined by Mach number, as it is for β_f and ϵ_d).

FUEL PUMP

The pressure ratio of the pump β_p can be related to the turbine expansion ratio β_t and the fan pressure ratio β_f, considering also the amount of pressure loss in the regenerative heat exchangers:

$$\beta_p = \frac{\beta_f}{\beta_t} \frac{p^0_{211}}{p^0_3} \frac{1}{\delta_{\text{HEX}}}, \tag{2.29}$$

in which the term δ_{HEX} represents the pressure loss that occurs to the fuel passing through the exchangers: it has been taken as an input to the fuel cycle [5], and maintained equal to 0.7 in subsonic regime, where the data were not enough. The turbine expansion ratio β_t is expressed as the ratio between the pressure at the inlet and at the outlet of the turbine:

$$\beta_t = \frac{p^0_5}{p^0_6} \tag{2.30}$$

With the pump pressure ratio, is possible to compute the pump power demand P_p in Eq. (2.31)

$$P_p = \dot{m}_{\text{LH2}} \frac{(\beta_p - 1) p_3^0}{\eta_p \rho_3^0} \tag{2.31}$$

defining completely the pump:

$$T_4^0 = T_3^0 + \frac{1 - \eta_p}{\eta_p} \frac{P_p}{(\dot{m}_3 C_{LH})} \tag{2.32}$$

$$p_4^0 = \beta_p p_3^0 \tag{2.33}$$

Regenerative Heat Exchangers

The heat exchangers are represented by their pressure loss and the entity of power extracted from the combustion chamber and the nozzle. For simplicity, they are both grouped under a single δ_{HEX} and a single quantity of extracted heat q_{HEX}. It is important to note the the hydrogen changes in phase while increasing in temperature, so it is considered in gaseous state. The Temperature and pressure are computed as follows:

$$T_5^0 = T_4^0 + \frac{q_{\text{HEX}}}{\dot{m}_4 c_{p,H2}} \tag{2.34}$$

$$p_4^0 = \varepsilon_{\text{HEX}} p_3^0 \tag{2.35}$$

The amount of heat extracted is imposed as an input: it has been taken initially from [5] for particular points in supersonic regime, and it has been retrofitted to extend the range of values. A more accurate model of the heat exchanger is in program.

Turbine

Passing to the turbine, it is represented in the scheme by two components, one dedicated to the fuel pump and one to the fan; in reality this is a single component that drives both pump and compressor, and the power requested to the turbine is set equal to the power demand by the pump and the fan:

$$P_t = P_f + P_p \tag{2.36}$$

where the fan power demand is computed in Eq. (2.37).

$$P_f = \dot{m}_{211} c_p (T_{31}^0 - T_{211}^0); \tag{2.37}$$

The turbine output is now completely defined:

$$T_6^0 = T_5^0 + \frac{P_t}{\dot{m}_5 c_{p,H2}} \tag{2.38}$$

$$\beta_t = \left[\left(\frac{T_6^0}{T_5^0} - 1 \right) \frac{1}{\eta_t} + 1 \right]^{-\frac{\gamma_{H2}}{\gamma_{H2} - 1}} \tag{2.39}$$

$$p_6^0 = \beta_t p_5^0 \tag{2.40}$$

It is remarkable to note that the fuel cycle is defined in a recursive way: the pressure ratio of the turbine depend from the pressure ratio of the pump, which depends in turn to the the expansion ratio of the of turbine again. For this motivation and for sake of calculation, since the results were promising, the pump pressure ratio was considered as an input: in [5] is possible to find the trend of β_p.

Combustion chamber

A strong limit to the previous model was the constancy of the fuel-to-air (FAR), limited to the stoichiometric value. This hypothesis puts a strong limitation relating the the modeling of varius flight condition and to the validation of the model itself. The dataset is complete enough to compute, for every point of the trajectory represented, the fuel-to-air ratio: this allows to tune the model in more realistic conditions. The fuel-to-air ratio is defined as:

$$f = \frac{\dot{m}_{\text{fuel}}}{\dot{m}_{\text{airl}}} \tag{2.41}$$

FAR is still an input to the model. This data provides the possibility to set the modeled engine in the same condition as expressed for each point in the trajectory (in term of Mach, altitude and FAR): in this way the results will be a direct index of the effectiveness of the implemented variations. In Fig. 2.10 is reported the optimized fuel-to-air ratio for each Mach and altitude (from VKI dataset) and the stoichiometric FAR $f_{\text{sto}} = 0.029$ maintained constant in the previous models: referring to the graph reported in Fig. 2.4,

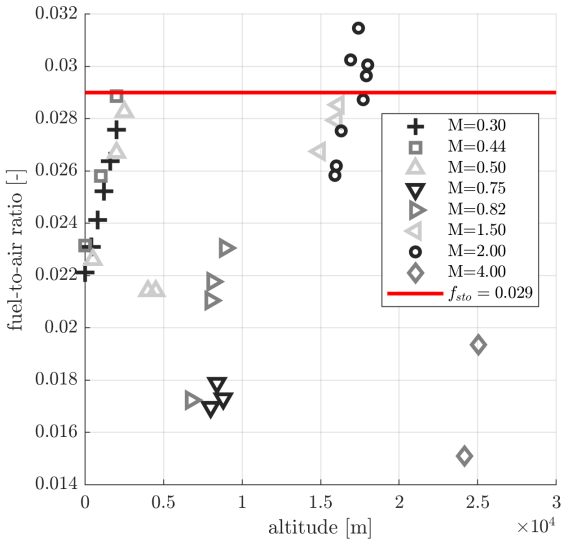

Figure 2.10. *Spread of the fuel-to-air ratio in the reference fligh conditions, compared to the stoichiometric value.*

it is understandable the reason because the errors on determined Mach could have been amplified : considering a constant f_{sto} consist in an over-estimation of the effective fuel-to-air ratio, producing a mismatch with the attended thrust. As it is still possible

to observe from Fig. 2.4 the error tends to lower values as the FAR is closer to stoichiometric value. Of course other factors, such as ε_d, β_f or C_x described earlier, influence the output: the optimal FAR at Mach 4 is distant from the stoichiometric, but the mismatch with the dataset is less than 10% during the vast majority of the trajectory.

The duty of the modeling of the combustion chamber is a good representation of the combustion process, in order to carry out the static values on injection temperature and pressure of the air before and after combustion. For this purpose it is necessary to know the geometry of the combustion chamber (especially the cross section). In [17] is possible to find a simple geometric scheme of the ATR burner: Using the corrected

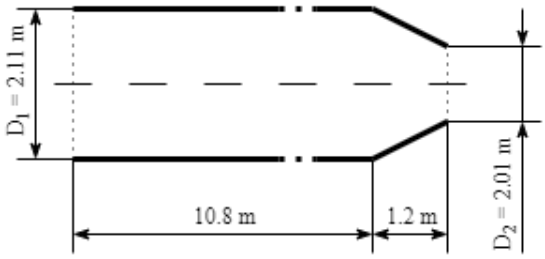

Figure 2.11. *Simple geometry scheme of ATR burner. Dimensions are rescaled.*

mass-flow to calculate the Mach number, the values of static T and P before combustion are calculated.

Nozzle

The expedient of treating the engine in subsonic regimes as a turbojet has been abandoned, considering the expansion after the combustion only along the nozzle. Following what exposed in Sec. 1.2.1 the fluidodynamic configuration inside the nozzle is complex, and it has been summarized in the behaviour of a converging-diverging nozzle (in Fig. 2.12 is reported the configuration in two operative conditions). The throat, which geometry is variable in relation at the consideration in [5], is always sonic, while the expansion in the diverging section consider the condition of non adapted nozzle: generally the exit pressure is different from the environmental pressure and $p_8 \neq p_0$. The under-expansion is not considered, since this condition does not occurs [5], while the over-expansion condition is taken into consideration by applying the *Summerfield* criteria, by which the exiting jet is considered detached from the nozzle wall if the pressure is as low as the 30% of the environmental pressure.

If Summerfield's hypothesis for fluid vein detachment occurs, the area ratio for

separation is computed via Eq. (2.42):

$$AR = \frac{\left(\frac{2}{\gamma'+1}\right)^{\frac{1}{\gamma'-1}} \left(\frac{p_8}{p_7}\right)^{-\frac{1}{\gamma'}}}{\sqrt{\frac{\gamma'+1}{\gamma'+1}\left[1-\left(\frac{p_8}{p_7}\right)^{\frac{\gamma'-1}{\gamma'}}\right]}} \tag{2.42}$$

and so the exit area is found through Eq. (2.43):

$$A_e = AR \cdot A_8 \ . \tag{2.43}$$

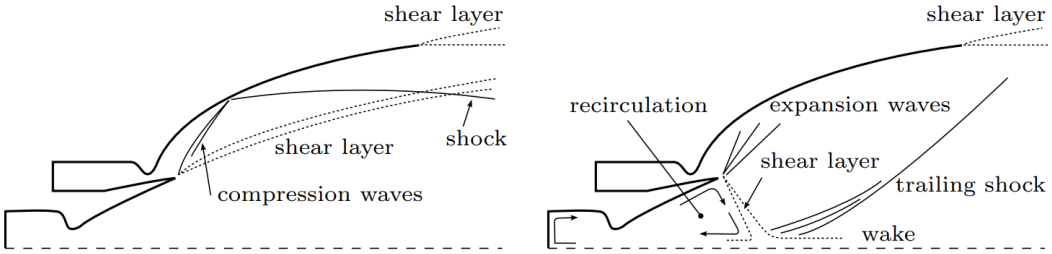

Figure 2.12. *Flow field in the nozzle, courtesy of [5].* [**1**] Both ATR and DMR active. [**2**] Only ATR discharging

2.4.2 Improvements of thrust modeling

Referring to some physical consideration about computing the output in term of thrust and specific impulse, Moino's model just considered the gross thrust over the net thrust, giving an approximation direct in the results themselves. Still referring to [15], is possible to give an approximation of the drag coefficient of the intake, referred the the frontal cross section of the aircraft. The drag coefficient, here indicated as C_x, is representative of the whole vehicle, and the generated resistance over thrust has to be scaled to a single ATR engine. Considering a flight regime where only ATR is operative, the drag will affect only the thrust generated by the modeled engine, so the effect over one of the six motors will be one sixth of the total drag. In Tab. 2.10 are reported some representative values for the C_x.

C_x Values					
Mach	1.5	2.0	3.0	4.0	4.5
$\mathbf{C_x}$	0.46	0.34	0.21	0.13	0.10

Table 2.10. *Known values of C_x at supersonic Mach numbers.*

Is now possible to calculate a virtual installed thrust for each motor as the uninstalled thrust minus the relative resistance:

$$\mathcal{T}_{\text{ATR's}} = \mathcal{T}_{u,\text{ATR's}} - \frac{1}{2}(\rho u^2)_0 A_0 C_x \tag{2.44}$$

where the uninstalled thrust T_u is evaluated as:

$$\mathcal{T}_{u,\text{ATR's}} = (\dot{m}w)_e + (p_e - p_0)A_e - (\rho u^2)_0 A_0 \alpha_{\text{c,LSI}} \tag{2.45}$$

The subscript e in Eq. (2.45) stands for the variables at the outlet, while the subscript 0 refers to the conditions at the inlet (station [*0*]).

2.4.3 Input of the updated model

In Tab. 2.11 are reported the input of the upgraded model. The core of the input is the same as the previous model, but the constant values referring to the performances of elements discussed in the previous section (highlited in bold-weighted font) are substituted with the coefficients of their relative interpolations. The coefficients, for sake of representability, are not reported.

ENGINE DATA			
Overall Pressure Ratio - Fan	$\beta_f(M_0)$	[-]	
Overall Pressure Ratio - Pump	$\beta_p(M_0)$	[-]	
Pneumatic Efficiency - Intake	$\varepsilon_d(M_0)$	[-]	
Pneumatic Efficiency - Combustor	ε_b	[-]	0.95
Pneumatic Efficiency - Heat Exchangers	$\eta_{\text{HEX}}(M_0)$	[-]	
Pneumatic Efficiency - Nozzle	ε_n	[-]	0.98
Adiabatic Efficiency - Fan	η_f	[-]	0.88
Adiabatic Efficiency - Combustor	η_b	[-]	0.90
Adiabatic Efficiency - Turbine	η_t	[-]	0.80
Mechanic Efficiency - Fan	η_{mf}	[-]	1.00
Mechanic Efficiency - Turbine	η_{mt}	[-]	0.95

PROPELLANT DATA			
Propellant storage temperature	T_3	[K]	20
Propellant storage pressure	p_3	[bar]	3
LH2 heat of reaction	H_i	[MJ/kg]	120.9
LH2 adiabatic expansion coefficient	γ_{LH}	[-]	1.5
LH2 specific heat	$c_{p,LH}$	[J/kgK]	14435
Stoichiometric fuel ratio	f_{sto}	[-]	0.029
Combusted adiabatic expansion coefficient	γ'	[-]	1.33
Combusted specific heat	c'_p	[J/kgK]	1900
Heat Exchangers subtracted heat	$q(M_0)$	[MW]	

GEOMETRCAL DATA			
Inlet Area	A_0	[m^2]	37.7
Combustion Chamber Area	A_{71}	[m^2]	3.5
Combustion Chamber Volume	V_{cc}	[m^3]	3.5
Outlet Area	A_{812}	[m^2]	20.6
Mass capture ratio	$\alpha_{c,\text{LSI}}(M_0)$	[-]	
Drag Coefficient	$C_x(M_0)$	[-]	

Table 2.11. *Input data for Updated Model.*

2.5 The aviable dataset

In this section is presented the dataset used to compare and analyze the goodness of the modeling. It is constituted by a series of performances and infra cycle data computed by the Von Kàrmàn Institute: some representative flight conditions, extrapolated from the trajectory analysis and described by Mach and altitude (in the firsts two columns, for each row), have been considered in a single point optimization. With this method, an optimal value for fuel and air mass flow rate is obtained, through which is possible to calculate the requested thrust reported in the third column.

In the lasts three columns are also reported the temperature of air, fuel and pressure (that is in common for both flows) before the ignition, in the combustion chamber; these values represent the magnitudes at the injection in the combustion chamber, and are far from the temperature and the pressure at the ignition. For a better understanding of the combustion process, a rapid overview is given in Sec. 3.1.

For each flight condition, constituting an input of the model in term of Mach number and altitude, this dataset will constitute a solid comparison base, allowing to regulate and tune each parameter in order to fit thrust, pressure and temperature before combustion in the best way possible.

STRATOFLY PROPULSIVE DATABASE: SUPERSONIC SPEED

Mach	**Altitude**	**Thrust**	**FUEL flow rate**	**AIR flow rate**	**FUEL Temp.**	**AIR Temp.**	**Pressure**
M	z	T	$\dot{m}_{\text{fuel}}$	$\dot{m}_{\text{air}}$	$T_{\text{air,71}}$	$T_{\text{fuel,71}}$	P_{71}
$[-]$	[m]	[MN]	[kg/s]	[kg/s]	[K]	[K]	[Pa]
1.5	14134.15	1.99	7.5	317.1	443	505	1.36E+05
1.5	14934.15	2.17	7.5	279.6	460	429	1.36E+05
1.5	16000	1.99	6.6	236.6	466	437	1.20E+05
1.5	16134.15	2.01	6.6	231.6	469	426	1.20E+05
2	15911	2.33	8.9	343.0	518	504	1.55E+05
2	16000	2.36	8.9	338.3	521	496	1.55E+05
2	16311	2.44	8.9	322.2	528	466	1.55E+05
2	16911	2.60	8.9	293.2	544	412	1.55E+05
2	17411	2.56	8.9	271.1	550	396	1.49E+05
2	17711	2.12	7.4	258.6	535	476	1.30E+05
2	17911	2.16	7.4	250.7	541	461	1.30E+05
2	18000	2.18	7.4	247.2	543	454	1.30E+05
4	24152	0.91	2.7	177.7	938	1019	3.43E+05
4	25052	0.96	3.0	154.4	963	1010	3.23E+05

Table 2.12. *Reference data from STRATOFLY MR3. Supersonic flight regime. The thrust is relative to the whole propulsion plant, and the thermodynamic variables are related to the injection in the combustion chamber.*

STRATOFLY PROPULSIVE DATABASE: SUBSONIC SPEED

Mach	**Altitude**	**Thrust**	**FUEL flow rate**	**AIR flow rate**	**FUEL Temp.**	**AIR Temp.**	**Pressure**
M	z	T	$\dot{m}_{\text{fuel}}$	$\dot{m}_{\text{air}}$	$T_{\text{air},71}$	$T_{\text{fuel},71}$	P_{71}
$[-]$	[m]	[MN]	[kg/s]	[kg/s]	[K]	[K]	[Pa]
0.30	0	2.31	8.9	401.4	363	542	1.90E+05
0.30	400	2.23	8.9	384.5	366	529	1.90E+05
0.30	800	2.14	8.9	368.1	368	517	1.90E+05
0.30	1200	2.07	8.9	352.3	370	505	1.90E+05
0.30	1600	2.02	8.9	337.1	372	492	1.90E+05
0.30	2000	1.99	8.9	322.3	375	479	1.90E+05
0.44	0	2.27	13.6	588.7	390	441	2.40E+05
0.44	1000	2.46	13.6	528.2	396	409	2.40E+05
0.44	2000	2.68	13.6	472.8	402	374	2.40E+05
0.50	500	2.42	14.3	633.9	398	414	2.51E+05
0.50	2000	2.80	14.3	537.2	407	361	2.51E+05
0.50	2500	2.94	14.4	507.8	410	340	2.51E+05
0.50	4000	2.30	14.3	669.0	395	430	2.51E+05
0.50	4500	2.31	14.3	669.0	395	430	2.51E+05
0.75	8000	1.13	6.6	390.1	395	430	2.51E+05
0.75	8400	1.21	6.6	370.1	358	248	1.20E+05
0.75	8800	1.08	6.0	351.0	351	258	1.10E+05
0.82	6750	1.44	8.6	500.7	376	523	1.55E+05
0.82	8000	1.22	7.3	347.9	361	542	1.16E+05
0.82	8121	1.23	7.4	342.6	363	472	1.18E+05
0.82	8921	1.30	7.0	306.3	363	444	1.12E+05

Table 2.13. *Reference data from STRATOFLY MR3. Subsonic flight regime. The thrust is relative to the whole propulsion plant, and the thermodynamic variables are related to the injection in the combustion chamber.*

Chapter 3

Pollutant emission evaluation

As it has been stated in the previous sections, the anthropogenic environmental impact, especially those concerning any kind of emissions, must be evaluated still from conceptual design phase. Nytrogen oxides constitute a severe source of environmental concerns indeed, at the same level of importance of carbon dyoxide emissions: the combustion products called nitrogen oxides, group to which NO and NO_x belong, are the major contributors to photochemical smog and the alteration of the O_3 levels; this last in particular results in a lack of ozone in the upper stratosphere, since NO_x participates in a chain reaction removing ozone from the atmosphere contributing to the ozone depletion, and therefore increasing the amount of harmful wavelengths of ultraviolet (UVB) reaching the Earth surface [18]. In this contest, cleared all the effects of the emission, directly or

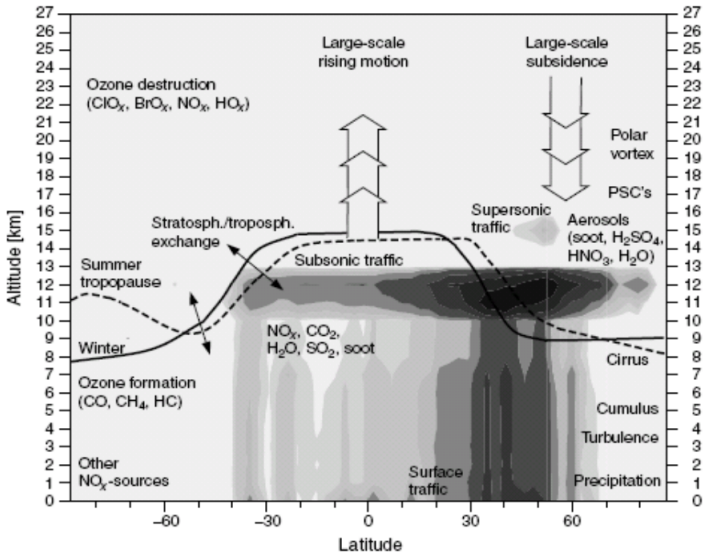

Figure 3.1. *[18] NO_x accumulation in the atmosphere at different altitudes and longitudes. The darker the shaded area the higher the NO_x emission rate.*

indirectly, of GHG and pollutant, the objective of this chapter is to analyze and describe the metodology that has been used to compute the emission database, on which it is

based the validation of the emissions previsions, and to present the $P_3 - T_3$ method; therefore NO_x will be treated as a unwanted side product of hydrogen and air combustion, and the emissions as will be evaluated in term of NO_x Emission Indexes ($EINO_x$), measured as grams of NO_x emitted per each kilogram of fuel burned. The emissions will be evaluated through 0D simulations which implements a kinetic mechanism that will model the combustion process and thanks to the $P_3 - T_3$ method: these results will be compared in order to extend the formulation of the $P_3 - T_3$ emission prediction method to supersonics engines fueled by hydrogen.

3.1 Hydrogen combustion

Hydrogen is a promising candidate as fuel for high-speed, air-breathing, trans-atmospheric, long-term passenger transportation aircrafts, since it can be burned in an efficient and reliable manner in supersonic combustion engines. Moreover, among the various available fuels, it possesses the highest heat release with the shortest kinetic time, wide flammability limits (4% – 75% by volume in air) and excellent cooling properties. On the other hand, due to the presence of zones of inverse dependence of reaction rate on pressure and its peculiar explosivity diagram, Fig. 3.2, the wide use of hydrogen powered engines may requires some technological improvements [19]. As it is possible to understand

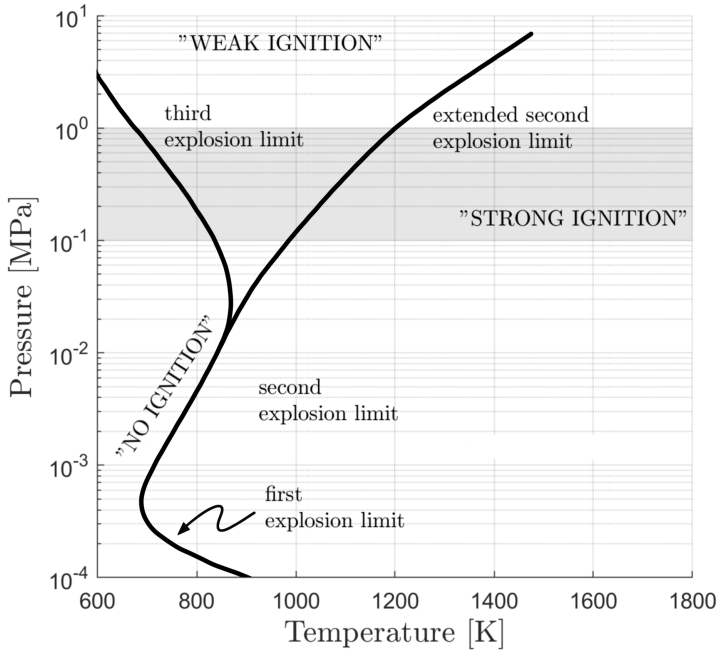

Figure 3.2. *Explosivity diagram of a H_2/air mixture.*

from its explosivity diagram in Fig. 3.2, the behaviour of the H_2 is much more sensitive on the temperature and pressure than conventional hydrocarbons, and its kinetic in term of characteristic time of the reaction is shorter than a carbon based molecule. On the

other hand, considering strictly about the number of reactions characterizing the combustion process, the description is easier: the hydrogen combustion could be detailed in about 30 reaction, unlike the combustion of an hydrocarbon which needs 320 reactions, or even a bio-fuel which needs in turn about 1000 reactions. In term of emissions,

H_2 COMBUSTION PARAMETERS		
Molecular weight	[a.m.u.]	2.016
Boiling point	[K]	20.268
Melting point	[K]	14.01
Density of gas @STP	[kg/m^3]	.0.0899
Specific heat @STP	[kJ/(kgK)]	14.304
Thermal conductivity @NTP	[W/(mK)]	0.187
Flammability limits in air	[vol %]	$4.0 \div 75.0$
Detonability limits in air	[vol %]	$13.0 \div 70.0$
Auto-ignition temperature in air	[K]	$793 \div 1023$
Gross heat of combustion or HHV	[kJ/mol]	286.1
Net heat of combustion or LHV	[kJ/mol]	241.7
Stoichiometric adiabatic flame temperature in air	[k]	2318
Laminar burning velocity	[m/s]	$2.65 \div 3.25$
Visible laminar flame speed	[m/s]	18.6
Detonation velocity	[m/s]	$1480 \div 2150$
Deflagration pressure ratio	[-]	8.15
Quenching distance @NTP	[m]	0.00064

Table 3.1. *Physical and chemical combustion parameters of hydrogen.*

and in particularly NO_xemission, in [13] is stated that using hydrogen as fuel can reduce emission; H_2 is a clean fuel since the overall product of its complete oxy-combustion is only water, even if, when reacts with air, it produces also NOx, due to the very elevated flame temperatures reached during combustion. In any case, the advantage of burning hydrogen from an environmental point of view is that it does not produce the greenhouse gas CO_2, neither any of the several other pollutant species i.e., CO, unburned hydrocarbons, Polycyclic Aromatic Hydrocarbons (PAH) and soot. Additionally, comparing H_2 to original carbon based fuels, the kerosene flammability region is smaller than that of hydrogen, which therefore will burn closer to the stoichiometric fuel-to-air ratio in order to maintain the stability: this will lead to high combustion temperatures, which will produce a larger amount of NO_x. However, hydrogen has a wider range of flammability and the entire operative range of the combustion may be shifted further into the lean region, as it can be seen computing the equivalence ratio of the ATR too, reducing the flame temperature and so the emissions. Furthermore, for its kinetic, hydrogen has an higher flame velocity if compared to kerosene; this allows a shorter combustor length and as a consequence a lower residence time: as it will shown further, since the kinetic of NO_xformation is slower, the relative reactions does not have the necessary time to

complete at the right temperature because the hot fluid is quenched exiting the thrust chamber. For the above-mentioned reasons, hydrogen is esteemed as a fundamental

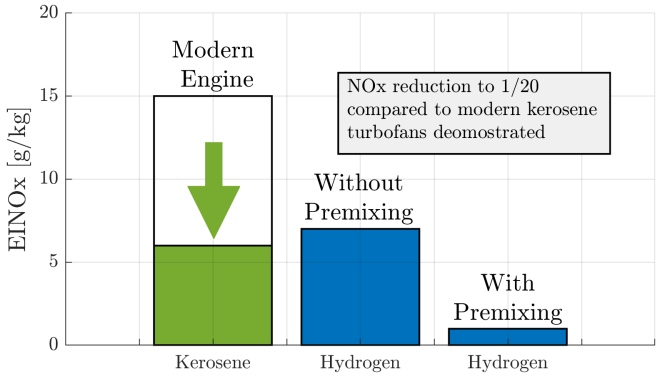

Figure 3.3. *[13]Comparison of NO_xemission for a gas turbine test setup applying H_2 or kerosene. Hydrogen quantity equivalent to kerosene quantity with the same energy.*

energy vector toward the decarbonized economy.

3.2 Mechanisms of NO_x formation

The formation of NO_x as a product of the majority of combustion processes is due to the chemical interaction of the air used as the oxidant. The atmospheric air is a mixture of gases, with a composition that varies along the altitude, and its mean composition is made up by the species reported in Tab. 3.2.

Species	Mole fraction	Species	Mole fraction
N_2	0.78	CH_4	1.72×10^{-6}
O_2	0.21	H_2	0.58×10^{-6}
H_2O	$2.5 \times 10^{-2} \div 3 \times 10^{-6}$	N_2O	0.31×10^{-6}
Ar	9.34×10^{-3}	CO	$0.06 \times 10^{-6} \div 0.12 \times 10^{-6}$
Ne	1.8×10^{-5}	O_3	$0.02 \times 10^{-6} \div 10 \times 10^{-6}$
He	5.2×10^{-6}		
Kr	1.1×10^{-6}		
Xe	9.0×10^{-8}		

Table 3.2. *The composition of the atmosphere.*

Three different mechanism, particularly relevant in air-breathing engine combustion, have been identified to generate the NO_x thorugh the interation with hydrogen, air and/or carbon-based molecules[1]:

[1]The fuel-bound nitrogen route (FBN) is not mentioned because it is mainly observed in coal combustion.

1. Thermal NO route.
2. NO prompt route.
3. N_2O route.

3.2.1 Thermal NO

The thermal NO mechanism, also called *Zeldovich NO* due to its recognition by Y. B. Zeldovich in 1946, is described by the following three elementary step reactions:

$$O + N_2 \longrightarrow NO + N \tag{3.1}$$

$$N + O_2 \longrightarrow NO + O \tag{3.2}$$

$$N + OH_2 \longrightarrow NO + H \tag{3.3}$$

while the global reaction is:

$$N_2 + O_2 \longrightarrow 2\ NO \tag{3.4}$$

The reaction (3.1) gives the "thermal" characterization of the method: it involves the breaking of the triple covalent bond in the N_2 molecule, a chemical process that requires an high thermal energy; for this reason this reaction is activated by high temperature, thus imposing a rate limitation on the mechanism [23]. This peculiarity will be particularly relevant defining the methods to limit the NO_x generation in combustion chamber, as highlighted in the last lines of the previous section.

3.2.2 Prompt NO

The mechanism of prompt NO, formulated by C. P. Fenimore in 1979 (and so called *Fenimore NO*), is an additional mechanism that describes the production of NO at the flame front. The reactions occur thanks to the interaction of nitrogen and the radical CH, which was considered an unimportant transient species. CH forms as an intermediate ad the flame front, and reacts with N_2, forming hydrocyanic acid (HCN), which reacts to NO in reaction (3.5) [23]:

$$CH + N_2 \longrightarrow HCN + N \longrightarrow \cdots \longrightarrow NO \tag{3.5}$$

Is important to note that the activation energy of the reaction (3.5) is 4.5 times lower that the same considered in the formation of thermal NO: for this reason prompt NO mechanism would still continue at lower temperatures.

The described mechanism occurs in presence of hydrocarbon combustion with air, especially under an hydrocarbon fuel, in the fuel-rich condition, that promotess the accumulation of C_2H_2 as a CH-prompt precursor. For these reasons, this mechanism is not so applicable in the reaction analyzed in this work.

3.2.3 Generation via N_2O

The *nitrous oxide N_2O mechanism* (formulated by Wolfrum in 1972) is similar to the reaction (3.2) in the thermal route, but considering the presence of a third body M generates N_2O, which in turn reacts to O, finally producing NO in reactions (3.6) and (3.7):

$$N_2 + O + M \longrightarrow N_2O + M \tag{3.6}$$

$$N_2O + O \longrightarrow NO + NO \tag{3.7}$$

The nitrous oxide mechanism is also particularly relevant with hydrocarbon fuels, when occurs a fuel-lean condition (suppressing the formation of CH and so the Fenimore NO mechanism) or low combustion temperature (suppressing the Zeldovich NO mechanism); this last condition is considerable when the first and simplest expedient cutting NO emissions through the limitation of Zeldovich route is implemented: lowering the temperature.

3.3 Kinetic mechanisms of H/O/N

In order to carry out an accurate modeling of the NO_x generated in a combustion process with hydrogen and air, needed further to compare the results obtained via P_3-T_3 method, a 0D kinetic analysis has been applied. The input is constituted by the mass fractions of the reactant, temperature and pressure at the injection, and the combustion has been simulated as exposed further.

3.3.1 Z22-NO_x20

This combustion scheme is a combination of a previously investigated hydrogen/oxygen kinetic mechanism i.e., Z22 [24], exhibiting a very satisfactory agreement between computational predictions and the experimental ignition delay times measurements up to a pressure of about 10 bar with a more complete NO_x generation reactions sub-mechanism. The kinetic mechanism details the hydrogen/oxigen combustion in 22 irreversible elementary reactions between 9 species. Referring to the hydrogen/air explosion diagram in Fig. 3.2, Z22 includes reactions for the complete temperature spectrum, below and above the crossover region. In particular, authors improved the capability of the scheme to match the ignition experimental behaviour also in the intermediate connecting region, an important zone considering the supersonic combustion engine.

Further is reported the mechanism in CHEMKIN format. Each reaction is correlated to its rate constant, depending from the temperature through the Arrhenius equation, Eq.

(3.8):

$$k = k_0 \mathrm{e}^{\frac{-\Delta E_A}{RT}} \tag{3.8}$$

where k_0 is a pre-exponential factor, ΔE_A is the activation energy, R is the universal ideal gas constant and T is the absolute temperature. The reactions that build up the mechanism are the followings:

$$\mathrm{H_2 + O_2 \longrightarrow H + HO_2} \qquad k = 7.40 \times 10^{05} \tag{3.9}$$
$$\mathrm{H_2 + M \longrightarrow H + H + M} \qquad k = 4.57 \times 10^{19} \tag{3.10}$$
$$\mathrm{HO_2 + H_2 \longrightarrow H_2O_2 + H} \qquad k = 3.00 \times 10^{06} \tag{3.11}$$
$$\mathrm{H + O_2 \longrightarrow OH + O} \qquad k = 2.45 \times 10^{14} \tag{3.12}$$
$$\mathrm{OH + O \longrightarrow H + O_2} \qquad k = 1.20 \times 10^{13} \tag{3.13}$$
$$\mathrm{O + H_2 \longrightarrow OH + H} \qquad k = 1.80 \times 10^{10} \tag{3.14}$$
$$\mathrm{OH + H \longrightarrow O_2 + H_2} \qquad k = 8.00 \times 10^{09} \tag{3.15}$$
$$\mathrm{H_2 + OH \longrightarrow H_2O + H} \qquad k = 1.17 \times 10^{09} \tag{3.16}$$
$$\mathrm{H_2O + H \longrightarrow H_2 + OH} \qquad k = 5.09 \times 10^{09} \tag{3.17}$$
$$\mathrm{OH + OH \longrightarrow O + H_2O} \qquad k = 6.00 \times 10^{08} \tag{3.18}$$
$$\mathrm{O + H_2O \longrightarrow OH + OH} \qquad k = 5.90 \times 10^{09} \tag{3.19}$$
$$\mathrm{H + O_2 + M \longrightarrow HO_2 + M} \qquad k = 1.80 \times 10^{18} \tag{3.20}$$
$$\mathrm{H + HO_2 \longrightarrow OH + OH} \qquad k = 1.50 \times 10^{14} \tag{3.21}$$
$$\mathrm{H + HO_2 \longrightarrow H_2 + O_2} \qquad k = 2.50 \times 10^{13} \tag{3.22}$$
$$\mathrm{OH + HO_2 \longrightarrow H_2O + O_2} \qquad k = 2.00 \times 10^{13} \tag{3.23}$$
$$\mathrm{HO_2 + HO_2 \longrightarrow H_2O_2 + O_2} \qquad k = 8.00 \times 10^{13} \tag{3.24}$$
$$\mathrm{H_2O_2 + M \longrightarrow OH + OH + M} \qquad k = 1.30 \times 10^{17} \tag{3.25}$$
$$\mathrm{OH + OH + M \longrightarrow H_2O_2 + M} \qquad k = 9.86 \times 10^{14} \tag{3.26}$$
$$\mathrm{H_2O_2 + OH \longrightarrow H_2O + HO_2} \qquad k = 1.00 \times 10^{13} \tag{3.27}$$
$$\mathrm{H_2O + HO_2 \longrightarrow H_2O_2 + OH} \qquad k = 2.86 \times 10^{13} \tag{3.28}$$
$$\mathrm{OH + H + M \longrightarrow H_2O + M} \qquad k = 2.20 \times 10^{22} \tag{3.29}$$
$$\mathrm{H + H + M \longrightarrow H_2 + M} \qquad k = 1.80 \times 10^{18} \tag{3.30}$$

3.4 0D kinetic simulations

Time-dependent 0D simulations of homogeneous, isochoric and batch reactors, filled with premixed, gaseous, reacting hydrogen/air mixtures were carried out using the kinetic and thermodynamic open-source Cantera software, developed by Prof. David Goodwin under Python interface, and the Z22-ZNOx20 kinetic mechanism developed

by the Swedish Defence Research Agency (FOI).

The kinetic simulation was carried out through the using of Cantera software [8] under Python interface.

The mathematical-chemical model consists in the following mass and energy balance equations:

$$m_{\text{tot}} = \sum_{k=1}^{K} m_k = \text{const.} \quad \Longleftrightarrow \quad \frac{\mathrm{d}m_{\text{tot}}}{\mathrm{d}t} = 0 \tag{3.31}$$

$$\frac{\mathrm{d}m_k}{\mathrm{d}t} = V r_k M_{w,k} \tag{3.32}$$

$$c_p \frac{\mathrm{d}T}{\mathrm{d}t} + v \cdot \sum_{k=1}^{K} (h_k r_k M_{w,k}) = 0 \tag{3.33}$$

The pressure of the reacting mixture was evaluated using the ideal gas law.

3.5 Prediction Techniques for NO_x Emissions

The prediction of NO_x emission is a complex and it is still beyond today's physical understanding and modeling capabilities [13]. The detailed prediction of NO_x emission involves, depending on the accuracy of the results and the available inputs, various modeling approaches along with different complexity.

It is possible to summarize and categorize the main methods present in the open literature in the following five families, in order of growing complexity [3]:

1. Emission correlation.
2. $P_3 - T_3$ method.
3. Fuel flow methods.
4. Simplified physics-based models.
5. High fidelity simulations.

3.5.1 Emission correlation

The emission correlation methods are based on the defining of characteristics parameters, that can be directly or indirectly correlated with the $EINO_x$. The correlation methods are further subdivided in two types of models: direct prediction and relative correlation, both based on engine data in term of performances and emissions obtained via combustor rig tests or engine tests at different flight conditions (i.e. SLS).

The direct methods consist of a formula which directly correlates $EINO_x$ to a set of engine parameters.

The relative correlation methods overcome the restrictions of the direct methods, and rely on publicly available data from, for example, ICAO database [13].

These models are the simplest to, but face some critical issues and have well noted disadvantages: the number of input is larger and they are difficult to obtain, especially for unconventional propulsive configurations, and the mathematical expression is sensitive to errors, also amplifying any of them if present in input data.

For these reasons, any emission correlation method has not been considered for the application to the case study.

3.5.2 $P_3 - T_3$ method

The $P_3 - T_3$ method is one of the simplest prediction methods present in open literature, and for its simpleness and effectiveness is largely used in the conceptual design phase. The core of the method, expressed in Eq. (3.34), it is based on the correction of the EI at sea level by using two variables taken from the combustion chamber: pressure at the ignition [10] and fuel-to-air ratio (FAR) at the ignition both at sea level and at flight level; the correction also depends on the effects of the atmospheric humidity, considered via the exponential H explicited in Eq. (3.35) in which h represents the specific humidity at the relative altitude in [$kg_{H2O}/kg_{dry\ air}$].

$$\text{EINOx}_{\text{FL}} = \text{EINOx}_{\text{SL}} \left(\frac{p_{3\text{FL}}}{p_{3\text{SL}}} \right)^{n} \left(\frac{\text{FAR}_{\text{FL}}}{\text{FAR}_{\text{SL}}} \right)^{m} e^{H} \tag{3.34}$$

$$H = 19(h_{\text{SL}} - h_{\text{FL}}) \tag{3.35}$$

The exponents showing in the equation are variable depending on the engine, but the majority of aeronautic engines fueled by conventional hydrocarbons could be considered $n = 0.4$ and $m = 0$.

Despite the simplicity of the method, it is still possible to observe some issues to its application: $P_3 - T_3$ method need proprietary and punctual data of the engine, such as pressure and temperature in the combustion, and the fuel-to-air ratio. Another relevant detail is that $P_3 - T_3$ is applicable to every engine by changing n and m indeed [3], but there is not a literature about, complicating the application to unconventional engine architecture.

The methodology is reported In Fig. 3.4 on the following page. It has to be followed in order to apply the $P_3 - T_3$ method, while the step by step process will be deeply defined further, in Sec. 3.6, being the $P_3 - T_3$ method the chosen one to predict ATR emissions.

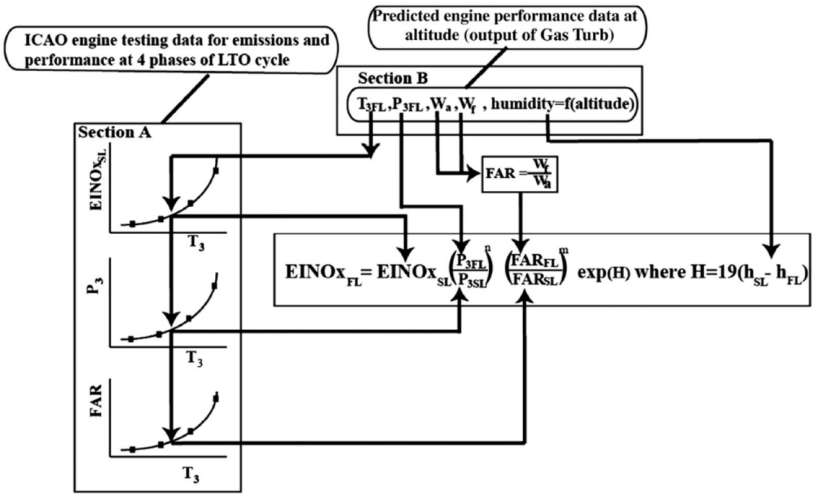

Figure 3.4. *Schematic of the methodology for the $P_3 - T_3$ method.*

3.5.3 Fuel flow

With the purpose of avoiding the necessity of proprietary data for $P_3 - T_3$ application, two similar methods are proposed: the BFFM2 (*Boeing Fuel Flow Method 2*) and the DLR fuel flow method, with the purpose to predict the emission indexes in a subsonic cruise condition.

Rather than using proprietary data, the method is based on public information present in the ICAO databank after an engine is certified, such as the Emission Indexes and the fuel flow during the four main phases of the flight, corrected with factors accounting installation losses.
Based on these data, the fuel flow in-flight is correlated with the fuel flow at sea-level; than the emission at sea level are correlated with the fuel flow, obtaining the Emission Indexes in generic flight conditions [4].

For BFFM2 the correlation between the fuel flow at flight level and sea level is reported in Eq. (3.36), while the correlation between the emissions is expressed in Eq. (3.37):

$$W_{f\text{SL}} = W_{f\text{FL}} \left(\frac{\vartheta_{\text{amb}}^{3.8}}{\delta_{\text{amb}}} \right) e^{0.2M^2} \tag{3.36}$$

$$\text{EINOx}_{\text{FL}} = \text{EINOx}_{\text{SL}} \left(\frac{\vartheta_{\text{amb}}^{1.02}}{\delta_{\text{amb}}^{3.3}} \right)^{0.5} e^{H} \tag{3.37}$$

where $\vartheta_{\text{amb}} = T_{\text{amb}}/288.15$, $\delta_{\text{amb}} = p_{\text{amb}}/101325$ and $H = 19(h_{\text{SL}} - h_{\text{FL}})$.

In literature is possible to find a mentionable variation to the canonical FFM, extending its application for supersonic aircrafts [7]. The study has been conducted correcting the hypothesis of an isoentropic flow between the freestream and the combustor in order to consider the supersonic field of motion, and considering the changes in the fuel lower heating value due to the kerosene blend with a biofuel. These considerations provided

to three correction factors: k_p for the pressure ratio, k_t for the temperature ratio and k_b to consider the fuel blend the blend, leading to a modified $EINO_x$ formula. The reformulation is reported in the next equation:

$$\text{EINOx}_{\text{FL}} = \text{EINOx}_{\text{SL}} \left[\frac{\vartheta_{\text{amb}}^{1.02}}{\delta_{\text{amb}}^{3.3}} \cdot k_p \left(\frac{p_{2\text{FL}}}{p_{1\text{FL}}} \right) \cdot \left(\frac{1}{k_t \dfrac{T_{2\text{FL}}}{T_{1\text{FL}}}} \right)^{3.3} \right]^{y} e^{H} k_b \tag{3.38}$$

3.5.4 Simplified physics-based models

The objective simplified physics models is to represent the combustion chamber combining reduced-order physics and chemistry model: the combustion chamber is virtually subdivided in different sections, each modeled as a combination of ideal reactors [3].

3.5.5 High fidelity simulations

Following this path, the numerical modeling of the flow is coupled to the advanced combustion and mixing physics modeling. These methods bring together all the complication of the computational problems: for exmple the complete geometry of the combustor is required for the application of the Reynolds-averaged Navier-Stokes equations in terms of boundary conditions.

Due to the different timescales and the physical phenomena involved, trying to maintain the accuracy of the modeling, direct numerical simulation for realistic combustion processes are non practical at the moment, with an excessive CPU-time for a fully 3D CFD simulation. Implementing Large-Eddy Simulation (LES) and cutting away the deep modeling of the small-scale turbulence, yet results in a lack of accuracy, a not suitable condition for an emission prediction tool.

3.6 Application of the $P_3 - T_3$ method

In this section the application of the $P_3 - T_3$ method was applied to the case study i.e., STRATOFLY ATR engines, examining all the complications of its implementation. As exposed earlier, the $P_3 - T_3$ method has been developed to describe and predict the emissions of an engine operating in subsonic regime and burning hydrocarbon fuel, so it is not surprising that its direct application will lead to ambiguous results that need to bee interpreted. Based on these firsts results from the direct application, analyzing the results, the achievement is the tuning of the method to the actual case study, trying to carry out a parallel formulation to represent an supersonic engine.

It is important to highlight that a direct comparison between the results of the $P_3 - T_3$ method application and an emission database is impossible, because an emission

database itself does not exist; as stated in the introduction, since STRATOFLY MR3 air turbo rocket is a concept, it is not present in any ICAO databank.

The adopted solution has been to first perform the simulation of the combustion process for each investigated point by means of the 0D kinetic simulation presented earlier. These data, considered as a reference, are directly compared to the results of the $P_3 - T_3$ method application.
The input of these simulation were constituted by the output of the engine model or by the points already present in the database, especially the values of temperature and pressure in combustion chamber. From this initial data, the emissions have been computed through the kinetic scheme named z22-NO_x20.

There is to say that a database was present in reserved literature, but the $EINO_x$ has been computed considering the mixing until it reaches the thermodynamic equilibrium temperature: this is the temperature reached by the mixture after a time tending to infinity, magnitudes higher than the characteristic time of the chemical kinetics of hydrogen and NO_x, and also way higher than the real residence time (not that after the residence time, the fluid expand in the nozzle and outside, immediately cooling itself, and the combustion does not proceed). Considering an infinite reaction time brings an over-estimation of all emission, in each flight condition. For these reasons the pre existing emission database was unservable, and the old has been completely recalculated. This process allowed

EINOx - original Emissive Database

Mach	**altitude**	**T injection**	**p injection**	**NOx Emission Index**
M [-]	z [m]	$T_{\text{air},71}$ [K]	p_{71} [Pa]	EINOx [g/kg]
0.33	0	363	1.90×10^6	**68.65**
0.40	0	390	1.90×10^6	**66.88**

Table 3.3. *EIcalculated at the equilibrium temperature for the known two points at sea level present in the original database. This method of emission index in not considered.*

on one hand to asses a first and reliable emissive database, computed ad-hoc to compare and validate the results from the application of $P_3 - T_3$ method, and on the other hand to obtain the emissions at sea level points of the flight envelope, required for using $P_3 - T_3$ in terms of $EINOx_{FL}$.

It is important to underline that the temperature and pressure necessary for the application of the $P_3 - T_3$ method are not the two values present in the propulsive database (under the name of T and p at the pre-ignition stage), but the respective values at the ignition. These two values refers to a specific instant in the combustion process, the ignition itslef. The combustion is a process of formation and propagation of radical species, that can be considered as divided in three macro phases: 1) the *initialization* (due to an abrupt augment of temperature or an electric spark), phase in which the first radical species are formed 2) the *chain ramification*, an exponential expansion of the radicals

(especially OH, the flame marker) and pressure and temperature rise 3) *termination*, in which radicals react and recombine to stable species. The ignition occurs during the initialization, after the ignition time delay, at that instant at which the concentration of the OH radical is at its maximum level (chemical ignition). In this specific instant the ignition values of temperature and pressure are detected, and the T_3 and p_3 to be used in the $P_3 - T_3$ method are computed.

So, the thermodynamic data present in the database, together with the air and the fuel mass flow, constitute the input of Cantera software, which will compute the profile of the mass fraction of the radical OH along time. This allows, through a spreadsheet algorithm, to individuate the peak of the mass fraction, instant at which T_3 and p_3 are calculated.

In 3.4 follows an example of the output of the process described: the computation as been carried for the known points at sea level, at Mach 0.30 and 0.44. The process has

EINOx - UPDATED EMISSIVE DATABASE

Mach M [-]	**altitude** z [m]	**T ignition** T_3 [K]	**p ignition** p_3 [Pa]	**NOx Emission Index** EINOx [g/kg]
0.33	0	2423.70	1.04×10^6	**2.12**
0.40	0	2449.53	1.34×10^6	**2.37**

Table 3.4. *EINOx calculated at the known two points at sea level present in the original database.*

been iterated intially for the whole available database, thus considering for each known flight condition the relative T_3, p_3 and EINO_x. After it has also been extended to some new conditions extrapolated by the ATR model developed in Chap. 1.3, extending the analysis to a wider range of Mach, still with limitations further described in Sec. 4 looking at the results.

However the input data necessary for the application of the $P_3 - T_3$ method has been carried out, so the canonical formulation i.e., using the exponents $n = 0.4$ and $m = 0$, as reported in Eq. (3.39) has been tried as first attempt. This formulation, as well as the others, has been applied to a specific Mach number, for which the condition at sea-level were evaluated.

$$\text{EINOx}_\text{FL} = \text{EINOx}_\text{SL} \left(\frac{p_{3\text{FL}}}{p_{3\text{SL}}} \right)^{0.4} \left(\frac{\text{FAR}_\text{FL}}{\text{FAR}_\text{SL}} \right)^{0} e^{H} \tag{3.39}$$

The errors are calculated as follows:

$$\text{Err } [\%] = \frac{\text{EINOx}_{P_3 - T_3} - \text{EINOx}_\text{ref}}{\text{EINox}_\text{ref}} \times 100 \tag{3.40}$$

As it will better explained in the Sec. 4.2, the direct application of the method does

not give promising result, thus the method in its original formulation, as expected, seems not to be applicable.
With the purpose to adapt the $P_3 - T_3$ method to a different class of engine, such as the ATR, in the following are analyzed alternative formulations to the classic one. In particular, is possible to investigate the influence of different exponents and linear factors: the value these coefficients is computed by retrofitting the reference data, in order to match the known values, using the *Curve Fitting toolbox* in MatLab®. In particular, the fitting consists in the adaptation of a particular fitting function based on two variables, i.e. $\mathbf{X}$ and $\mathbf{Y}$, and the relatives coefficients to determine fitting the values in Z. The relationship is power law-like, similar to Eq. (3.41):

$$Z = a \cdot X^b \cdot Y^c \tag{3.41}$$

The Eq. (3.41) should fit the various formulation of the $P_3 - T_3$ mothod, and the coefficients a has to be considered comprehensive of the whole multiplicative factors of the variables attributed to X and Y.

Adding just a multiplicative factor a, as expressed in Eq. (3.42), does not give substantial variations, since the errors is still great and the R-square[2] of the fitting is lower than 1.

$$\text{EINOx}_{\text{FL}} = a \cdot \text{EINOx}_{\text{SL}} \left(\frac{p_{3\text{FL}}}{p_{3\text{SL}}}\right)^{0.4} \left(\frac{\text{FAR}_{\text{FL}}}{\text{FAR}_{\text{SL}}}\right)^{0} e^{H} \tag{3.42}$$

Since the combustion process of the hydrogen is more sensitive to the pressure than the same for an hydrocarbon, for example kerosene (the fuel for which the $P_3 - T_3$ method has been conceived) the p_3 ratio should have an higher weight in the whole formulation, and the exponent $n = 0.4$ should be changed. Following this path, a more complete formulation, reported in Eq. 3.44, has been tried: it implements a variable p_3-ratio coefficient, named b, as well as the multiplicative coefficient a:

$$\text{EINOx}_{\text{FL}} = a \cdot \text{EINOx}_{\text{SL}} \left(\frac{p_{3\text{FL}}}{p_{3\text{SL}}}\right)^{b} \left(\frac{\text{FAR}_{\text{FL}}}{\text{FAR}_{\text{SL}}}\right)^{0} e^{H} \tag{3.43}$$

With this approximation the results are more encouraging, as discussed in Sec. 4.2.

Two variations of increasing complexity has been tested, trying to taking in account the influence of the fuel-to-air ratio considering the term $\text{FAR}_{\text{FL}}/\text{FAR}_{\text{SL}}$ powered to a

[2]R-square is known as the coefficient of determination, and indicates to proportionate amount of variation in the response variable y explained by the independent variables x in the linear regression model. So, the larger the R-square is, the more variability is explained [14].

constant exponent 1 (Eq. (3.44)) and to an exponent c (Eq. (3.45)).

$$\text{EINOx}_{\text{FL}} = a \cdot \text{EINOx}_{\text{SL}} \left(\frac{p_{3\text{FL}}}{p_{3\text{SL}}} \right)^{b} \left(\frac{\text{FAR}_{\text{FL}}}{\text{FAR}_{\text{SL}}} \right) e^{H} \tag{3.44}$$

$$\text{EINOx}_{\text{FL}} = a \cdot \text{EINOx}_{\text{SL}} \left(\frac{p_{3\text{FL}}}{p_{3\text{SL}}} \right)^{b} \left(\frac{\text{FAR}_{\text{FL}}}{\text{FAR}_{\text{SL}}} \right)^{c} e^{H} \tag{3.45}$$

Chapter 4

Results and Discussions

4.1 ATR modeling

4.1.1 Upgraded model

The improvements implemented on the pre-existing ATR model exposed in Sec. 2.3 has been analyzed in terms of thrust and therodynamic variables, the most suitable variables for the comparison. Thus the output will be analyzed and discussed, evaluating the effectiveness of the improvements through a direct comparison with the aviable database described and reported in Sec. 2.5.

The following comparative graph are structured as follows: each black cross point represents every row reported in the database in terms of the analyzed variable and altitude, grouped in function of the Mach number. The colored markers represents instead the same variable at the same condition, as evaluated by the upgraded model; the value of both data can be read on the right y-axis. In the background of the graph the grey bars represent the error between the computed thrust and the reference data, calculated by means of Eq. (3.40); the value of the error can be read on the left y-axis, where its percentage is reported.

Analyzing the thrust, in Fig. 4.1 and 4.2 on the next page are reported the errors resulting by implementing the changes in the initial air cycle, that is the fitting of $\varepsilon_d(M_0)$ and $\beta_f(M_o, z)$. This upgrade has significantly improved the original models, since the previous approximation imposed on the pressure ratio and the total pressure recovery were the most restricting. Comparing the obtained errors with the original complete model presented in Sec. 2.3, the mismatch at low-subsonic Mach numbers reduced considerably: before the error at Mach 0.30, 0.44 and 0.50, at the trajectory flight level, were fluctuating from 60 to peak of 180%, while it is now settled among the 20%, with a maximum peak of circa 30% (Fig. 2.4).

The worst errors are now found in high subsonic Mach numbers, such as 0.75 and 0.82, while the output in supersonic regime reduced the mismatch, except for Mach

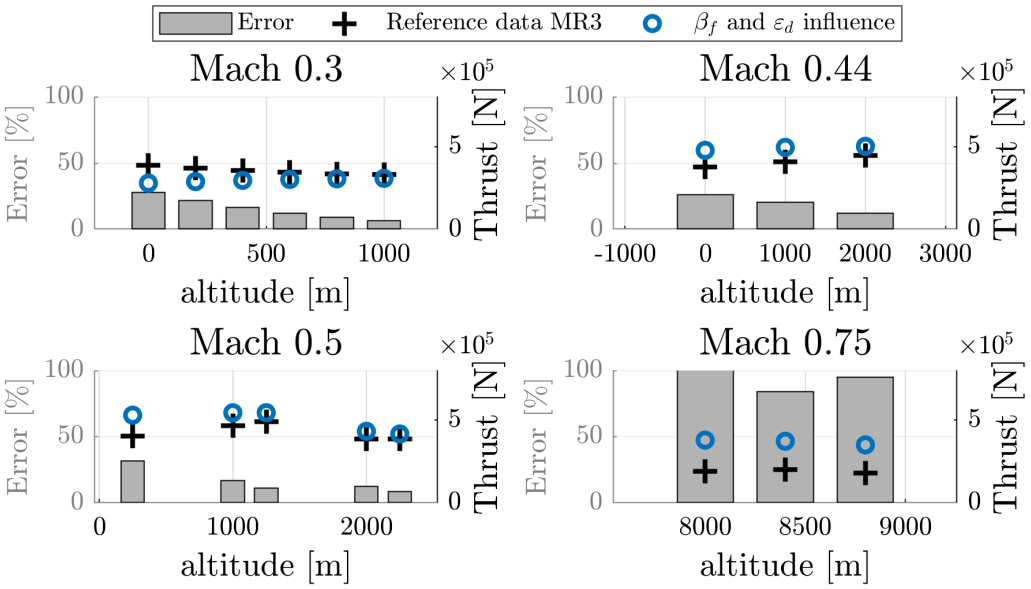

Figure 4.1. *Impact of β_f and ε_d in the thrust calculations. Mach = 0.30; 0.44; 0.50; 0.75.*

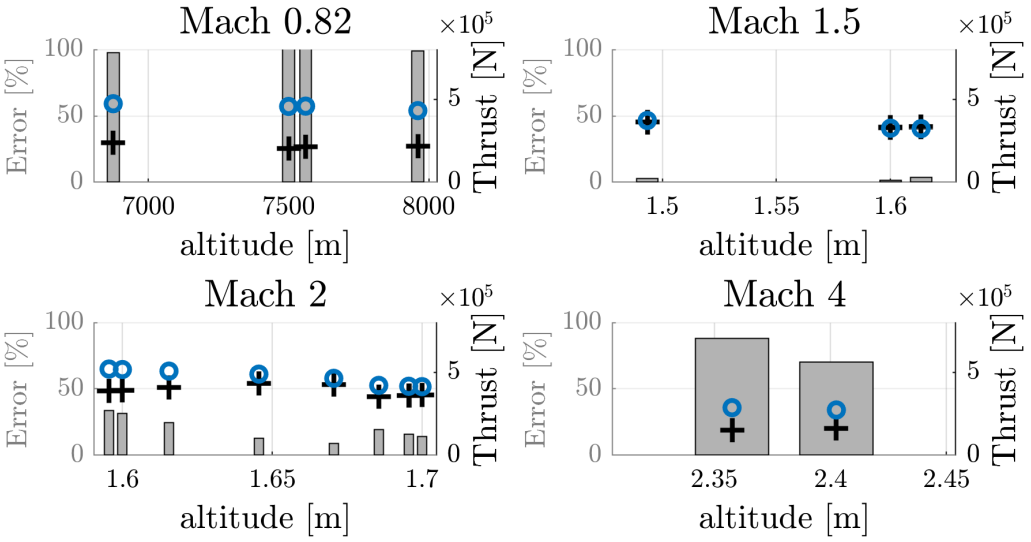

Figure 4.2. *Impact of β_f and ε_d in the thrust calculations. Mach = 0.82; 1.50; 2.00; 4.00.*

4.0. In general the error lowered a in sensitive part of the trajectory, not encountering anymore peaks as found in the previous model.

Thank to the propulsive database it is also possible to look at the errors arising from the mismatch with the conditions in the combustion chamber in terms of pressure before combustion (Fig. 4.3 on the facing page), the station [*71*] in the engine model. This allows to better understand the propagation of the error through the calculations of the various stations composing the model. Observing the following graph, in which are reported the most problematic Mach numbers in term of p_{71}, there is generally an amplification of the error: observing for example Mach 0.75 in Fig. 4.3 the error on

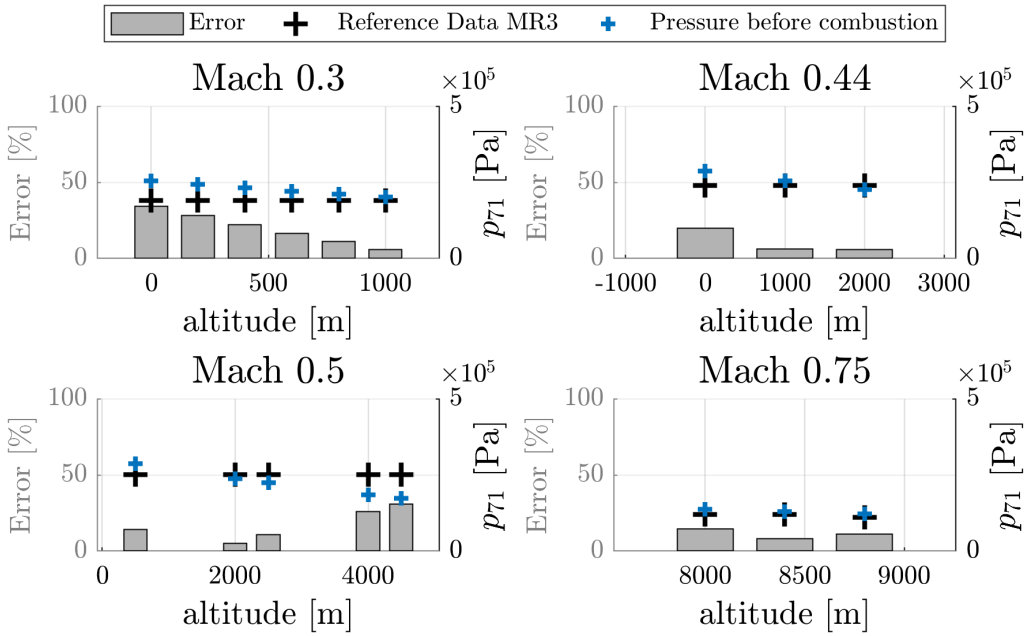

Figure 4.3. *Errors on the pressure before combustion* p_{71}

parameters before combustion is lower than the error on the thrust output.

The behaviour of the temperature before combustion T_{71} is more regular, as reported in Fig. 4.4 and 4.5 on the following page, except for the points at Mach 4, that should need a more detailed insight:

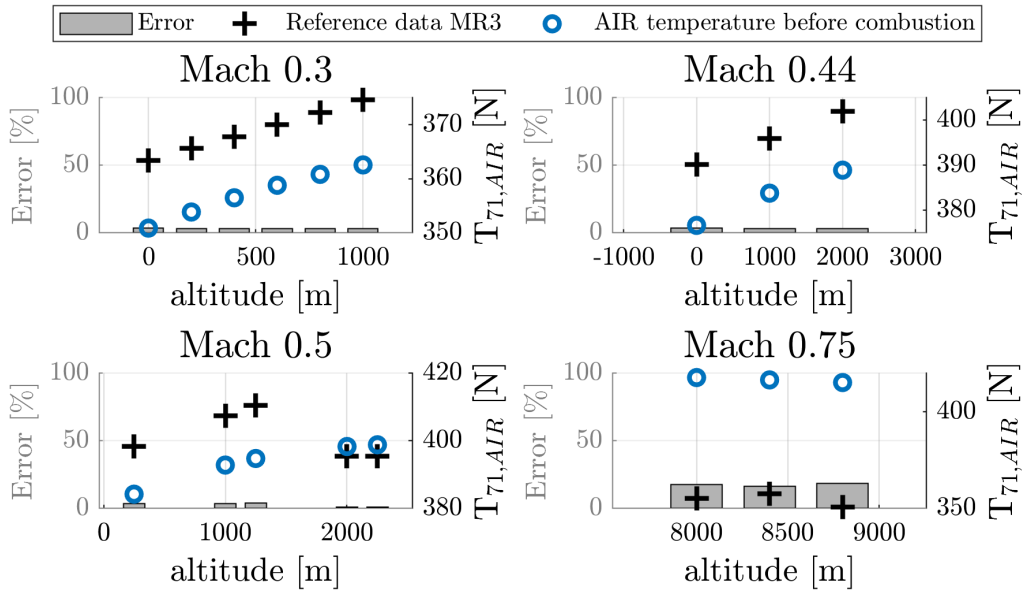

Figure 4.4. *Errors on the temperature before combustion* T_{71}.

Based on the the graphs presenting *de facto* only the errors from the air cycle, some other mismatch could be hidden in the calculations of the combustion process or the expansion in nozzle. The implementation of the upgraded model of the nozzle and

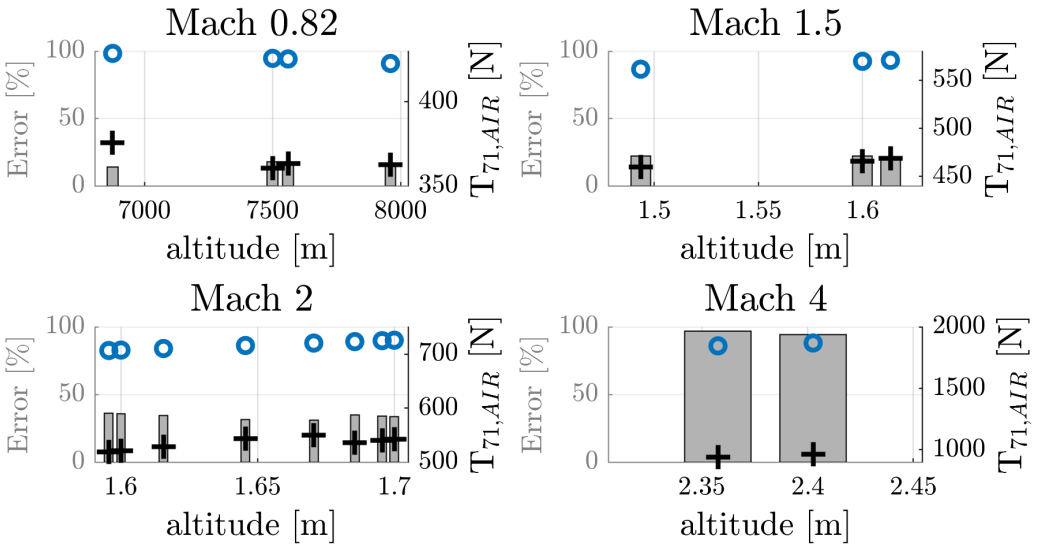

Figure 4.5. *Errors on the temperature before combustion T_{71}.*

considering the installed thrust brought to the following results in Fig. 4.6 and 4.7 on the next page: The result reported in the graph of the upgraded model are promising,

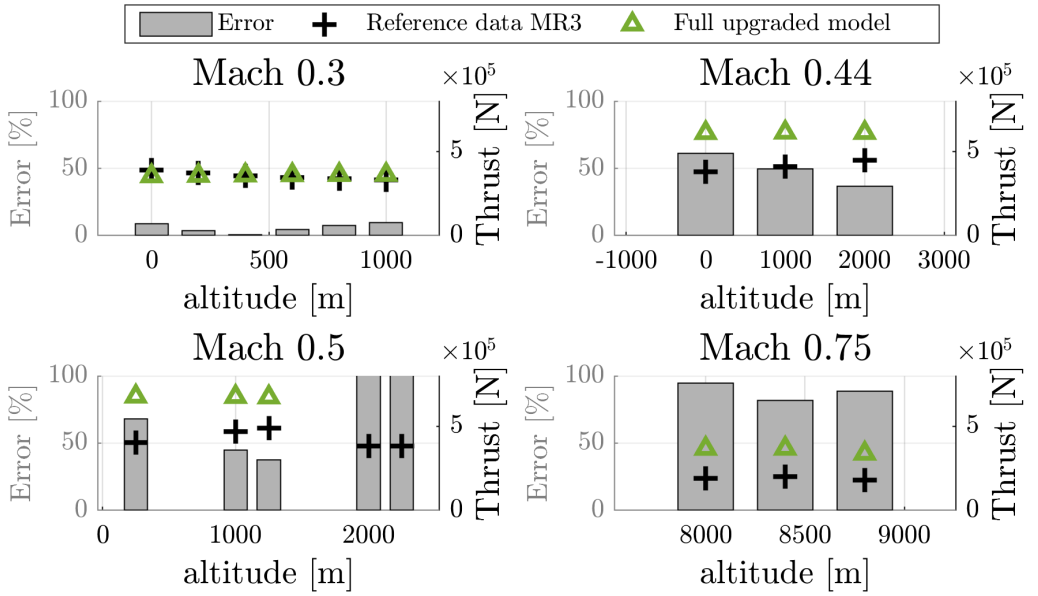

Figure 4.6. *Results of the full upgraded model compared to the propulsive database. Mach = 0.30; 0.44; 0.50; 0.75.*

except for the subsonic Mach numbers. In literature are found some calculation made by Dr. Guido Saccone from CIRA, presented in the framework of STRATOFLY Progress Meeting n.4 [17], in which are reported the calculations of the cinematic variables at the injection, reported in Tab. 4.1:

In most of the cases the injection velocity is supersonic, and this could influence the combustion, not modeled as a supersonic combustion in the reference data. This could lead to some errors affecting the propulsive database.

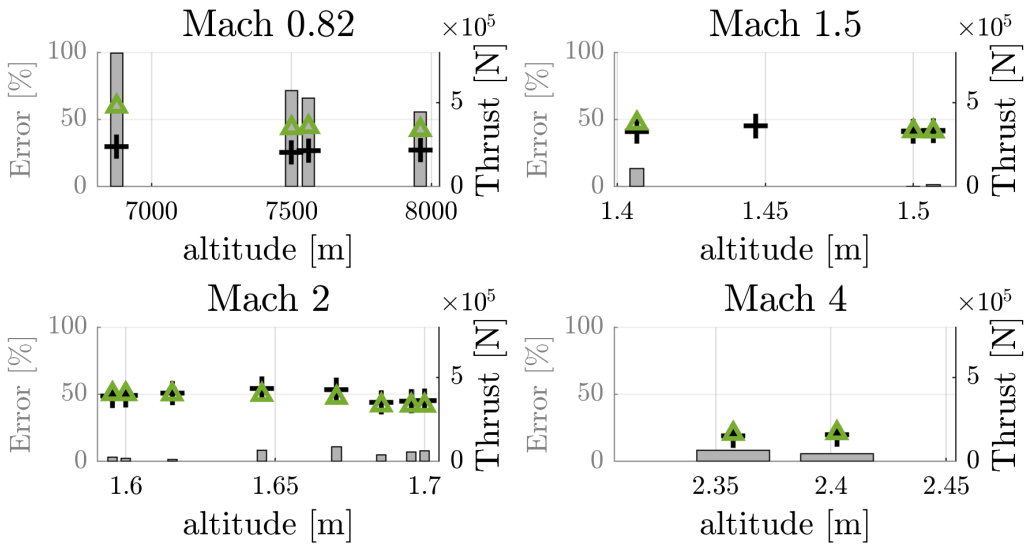

Figure 4.7. *Results of the full upgraded model compared to the propulsive database. Mach = 0.82; 1.50; 2.00; 4.00.*

INJECTION MACH NUMBERS BY CIRA

Mach M [-]	**velocity** v [m/s]	**Sound speed** a [m/s]	**Mach inj.** $M_{\text{inj.}}$ [-]
0.30	432.346	437.215	0.989
0.44	561.597	432.090	**1.300**
0.50	566.908	432.280	**1.311**
0.75	565.366	427.980	**1.321**
0.82	553.341	392.770	**1.409**
1.50	565.584	453.680	**1.247**
2.00	583.416	481.730	**1.211**
3.00	463.266	585.800	0.791
4.00	102.379	623.850	0.164
4.50	82.455	685.680	0.120

Table 4.1. *Injection Mach number as computed by CIRA. The bolded values refer to a supersonic Mach.*

In the following is presented a direct comparison between the upgraded and the previous reference model. Since the second is tuned to work in stoichiometric conditions, the calculations on thrust are made imposing as an input to the upgraded model a fuel-to-air ratio equal to stoichiometric. This process allows to have a global view to the beahiour of the new model in relation to the thrust otput. The direct comparison shown in Fig. 4.8 on the following page reveals that the relative results differ for less than 10%, asserting that the model present in literature under-extimates the thrust at the majority of Mach numbers. However the most important upgrades consist in the calculation of the infra-cycle variables, necessary to the application of the $P_3 - T_3$ method.

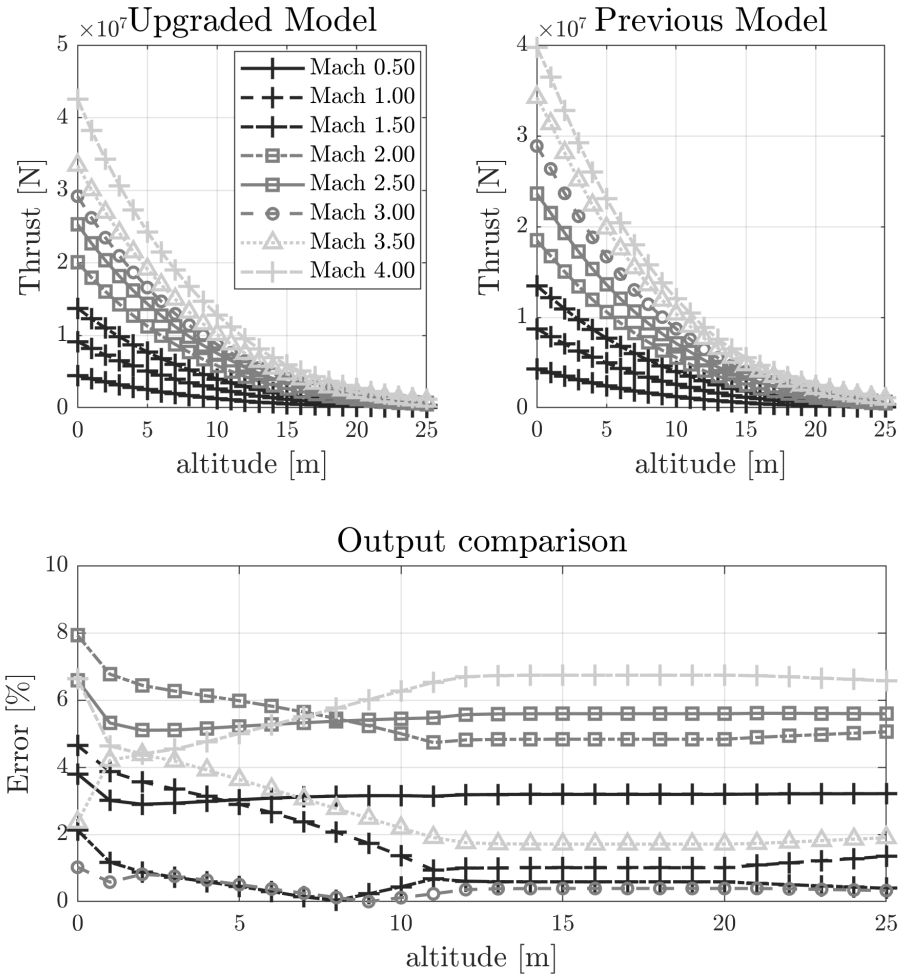

Figure 4.8. *Direct comparison on the output between the upgraded model and the literature most model, at* $\phi = \phi_{sto} = 1$.

4.1.2 Propulsive maps

The upgraded numerical model refined in Sec. 2.4 still has a degree of freedom besides the number of Mach and the altitude, as the fuel-to-air ratio constitute an input to the calculation. For this reason, it is not possible to obtain the behaviour of the thrust output in a specific flight condition given the flight level and the speed, since the value of the equivalence ratio should be earlier identified. Some strategies, presented further, has been identified to overcome this problem.

In Fig. 4.9 is reported the the thrust for various Mach numbers, covering the trajectory of STRATOFLY where the ATR is active, for a range values of the Equivalence Ratio ϕ that represent fuel lean and rich conditions. The equivalence ratio is defined in Eq. (4.1):

$$\phi = \frac{f}{f_{\text{sto}}} \quad . \tag{4.1}$$

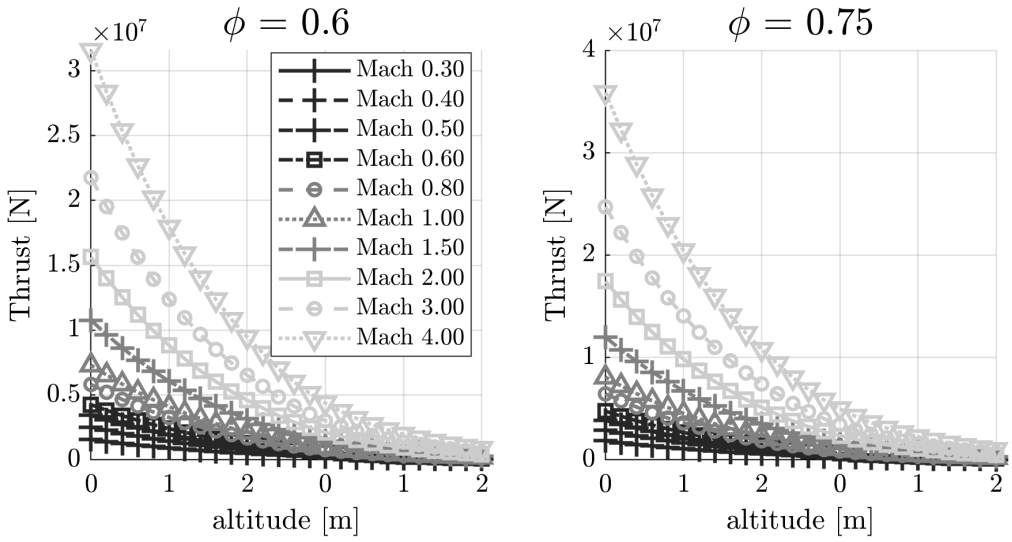

Figure 4.9. *Propulsive performances for different values of equivalence ratio, in a wide range of Mach and altitude.* $\phi = 0.6$ *and 0.75.*

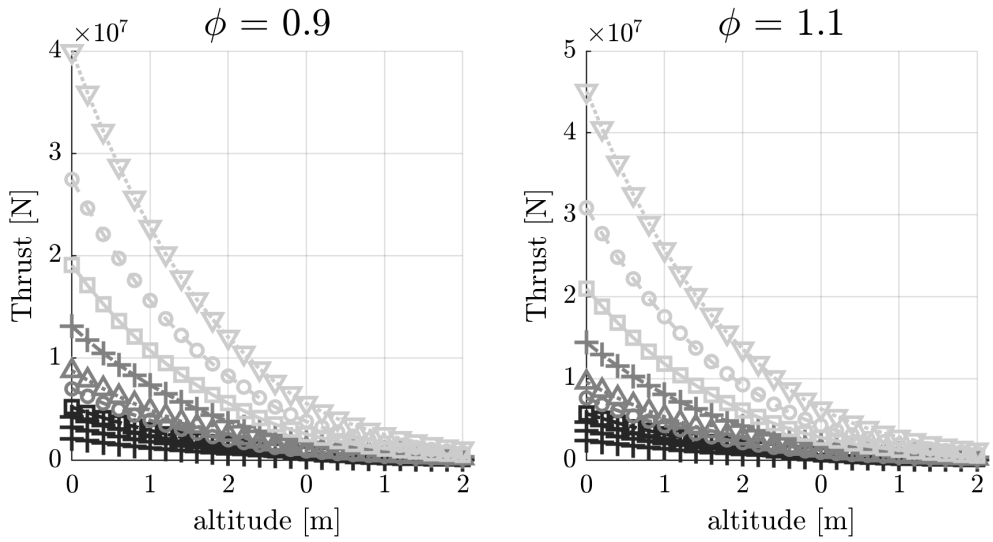

Figure 4.10. *Propulsive performances for different values of equivalence ratio, in a wide range of Mach and altitude.* $\phi = 0.9$ *and 1.1*

To obviate the problem of the fuel-to-air ratio the mission profile needs to be determined: knowing the mission profile in term of necessary thrust at a specific Mach and altitude corresponds to a precise value of equivalence ratio; thus is possible to compute, imposing it as an input to the model, the performances and the engine data in the considered flight condition. This process is be similar to choose a determine a specific point in the map presented in Fig. 4.11, 4.12 and 4.13, which for various Mach numbers (in the graphics are reported the representative values already present in the propulsive database), the performances are computed ranging over different equivalence ratio from fuel-lean to mixtures, and their values refer to the side colorbar.

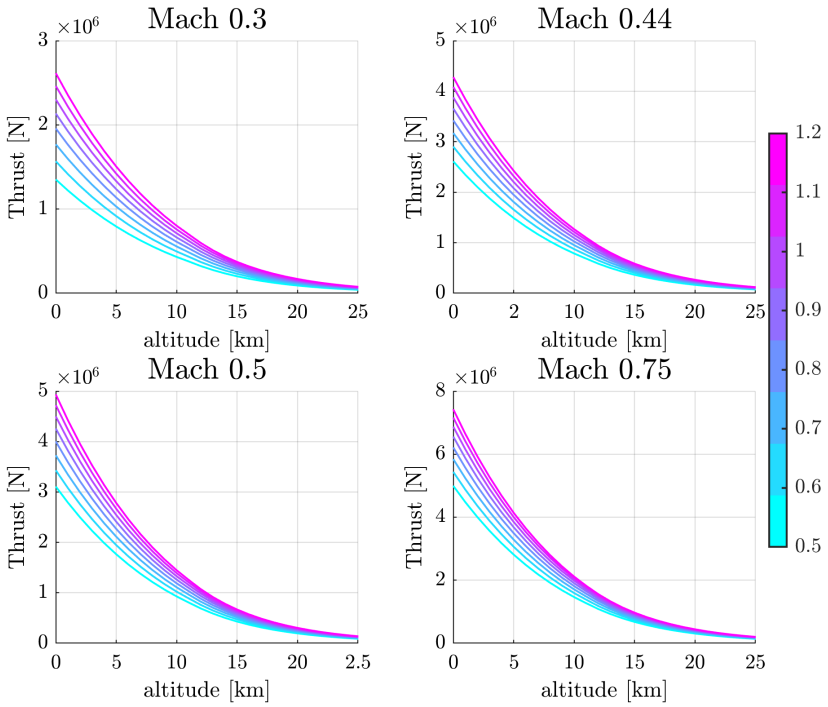

Figure 4.11. *Thrust map of the engine model, with varying equivalence ratio, in subsonic conditions.*

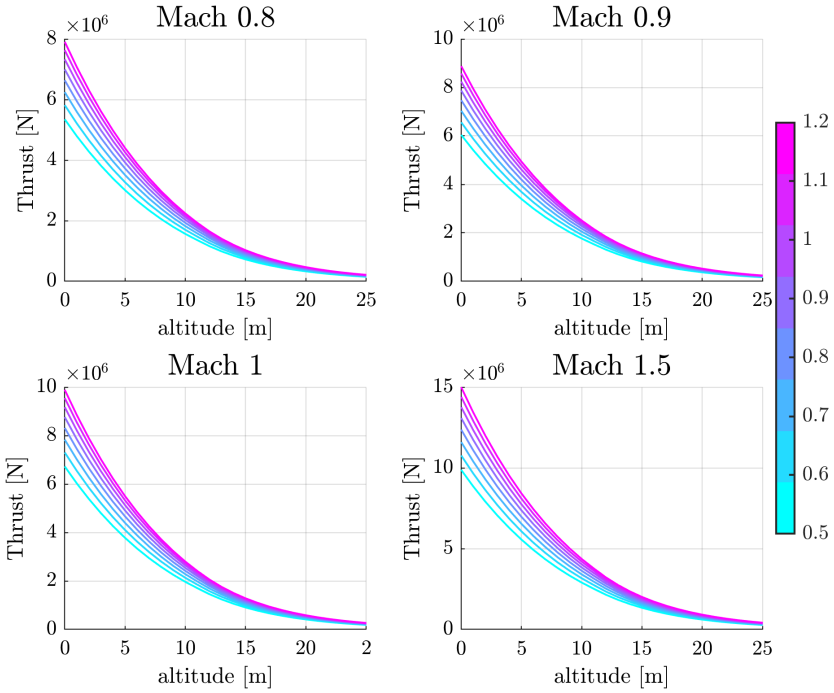

Figure 4.12. *Thrust map of the engine model, with varying equivalence ratio, in transonic and supersonic conditions.*

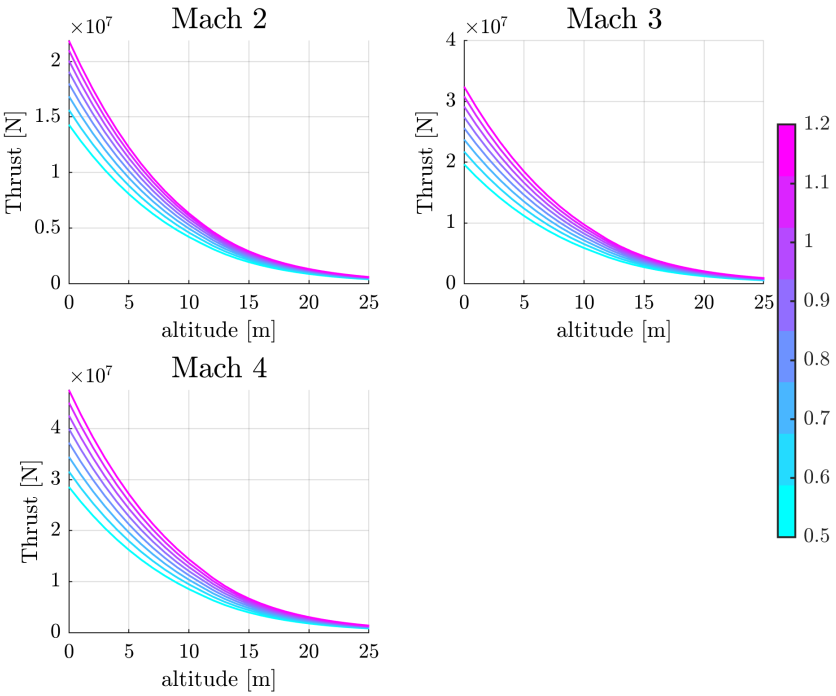

Figure 4.13. *Thrust map of the engine model, with varying equivalence ratio, in supersonic conditions.*

Another option in the determining the fuel-to-air ratio would be to indentify a value to minimize the NO_x. [12] analyzed the combustion process in the LAPCAT II MR2.4, in particular the influence of equivalence ratio and pressure in the production of NO_x. In particular, the equivalence ratio influences the adiabatic flame temperature, that has its peak for $\phi = 1.2$, while the peak of emissions is for $\phi = 0.8$ for a residence time of 10 ms. Shifting to a more realistic residence time of t = 0.07 ms, the peak of NO_x is for $\phi = 1.3$ and is found a greater reduction for lean mixtures. According to the ICAO databank [11] and to [12], an equivalence ratio of 0.6 brings NO_x emissions within axceptable amounts (less than 50 ppm).

Comparing the FAR corespondent to the equivalence ratio found by [12] with the values in the propulsive database, optimized for each condition, seems that a realistic fuel-to-air ratio is for richer mixtures. In Fig. 4.14 is reported the value of the equivalence ratio at each known flight condition (black cross), compared to $\phi = 0.6$ as found in [12] (red line).

Anyway imposing $\phi = 0.6$ results in a reduction of the thrust, output that should be compared with the necessary thrust at that specific Mach and altitude, in order to ascertain if the imposed FAR could be effective.

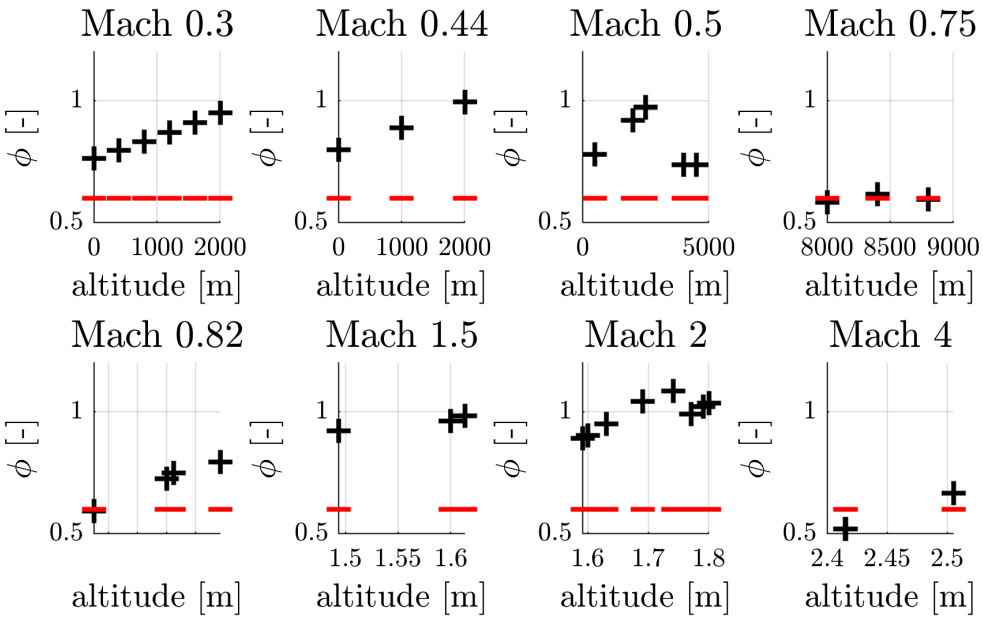

Figure 4.14. *Velues of the equivalence ratio ϕ at each know flight condition, compared to the optimal value found [12]*

4.2 Emissions modeling

4.2.1 Original database

The various versions of the $P_3 - T_3$ method presented in Sec. 3.6 have been applied initially at the subsonic Mach conditions described in the propulsive database computed by VKI, which has been enlarged with some point at sea level (approximating the fuel-to-air ratio) and each enriched with the temperature and the pressure at the ignition.

As it is possible to observe in Fig. 4.15, the original formulation (blue dot) is in not agreement with the database, while the variations presents low errors for all the fitting, yet still having some derives in the yellow points for Mach 0.5. The first approximation (Eq. (3.42)), due to the fitting problems already described in term of R-square, has not been reported. In Tab. 4.2 is reported a first overview of the exponents found along the

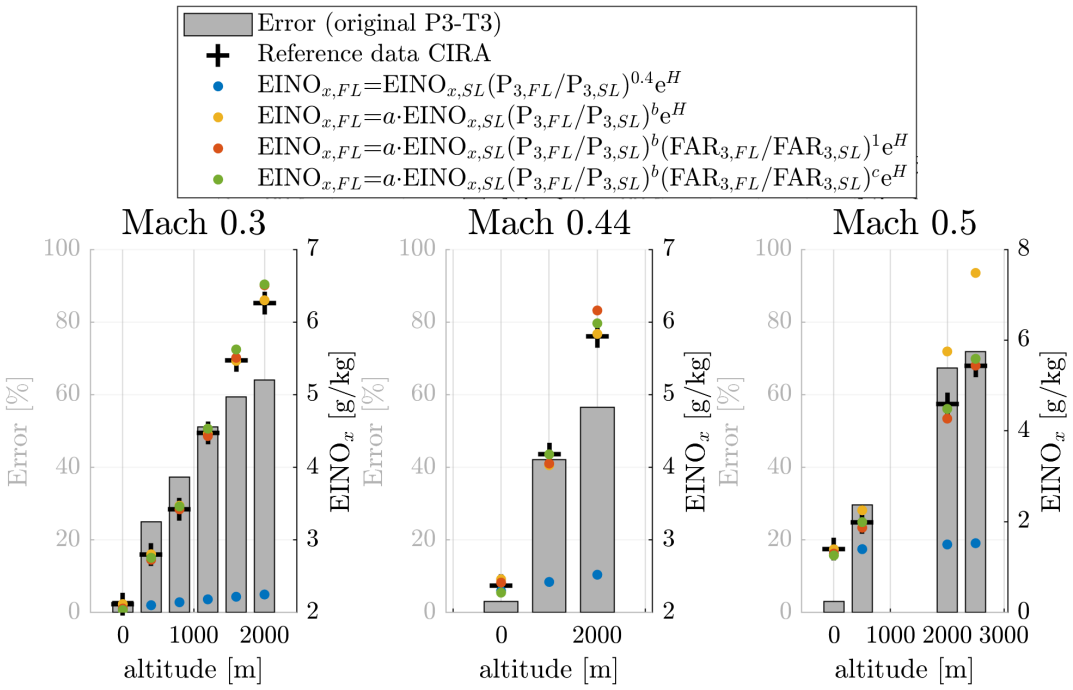

Figure 4.15. *Results of the application of the $P_3 - T_3$ method in its original formulation and in all its declinations. The errors refers only to the canonical formulation of the method. A complete list of the errors is reported in Tab. 4.2.1.*

application of the various declinations of the $P_3 - T_3$ method, while in Tab. 4.2.1 are reported the errors calculated in the application of the canonical formulation, along the errors computed applying the other formulations of the method: Analyzing the results, in particular the values of the a, b and c interpolation coefficients, some conclusions could be carried out:

- The coefficient a is always close to the value of 1 in the range of Mach analyzed. Despite the case analyzed is still a bit unrealistic, and a seems to decrease

	$P_3 - T_3$ VER. 2		$P_3 - T_3$ VER. 3		$P_3 - T_3$ VER. 4		
Mach	**a** coeff.	**b** coeff.	**a** coeff.	**b** coeff.	**a** coeff.	**b** coeff.	**c** coeff.
0.30	1.03	22.28	1.00	18.80	0.99	24.98	-0.23
0.44	1.07	15.13	1.05	12.30	0.99	30.69	-3.23
0.50	1.03	14.03	0.96	11.89	0.93	17.3	-0.76

Table 4.2. *Factors found in the application of the variations of the $P_3 - T_3$ method to the low-subsonic points reported in the original propulsive database.*

		REF.	ORIG. $P_3 - T_3$		VER. 2		VER. 3		VER. 4	
M	**z**	**EINO$_x$**	**Err.**	**EINO$_x$**	**Err.**	**EINO$_x$**	**Err.**	**EINO$_x$**	**Err.**	**EINO$_x$**
[−]	[km]	[g/kg]	[%]	[g/kg]	[%]	[g/kg]	[%]	[g/kg]	[%]	[g/kg]
0.30	0	**2.12**	3.03	2.1	0.12	2.1	3.03	2.1	4.00	2.0
0.30	0.4	**2.80**	24.93	2.1	0.12	2.8	2.56	2.7	1.74	2.8
0.30	0.8	**3.42**	37.34	2.1	1.54	3.5	0.07	3.4	0.97	3.5
0.30	1.2	**4.47**	51.16	2.2	0.16	4.5	0.88	4.4	1.04	4.5
0.30	1.6	**5.47**	59.44	2.2	0.09	5.5	0.69	5.5	2.32	5.6
0.30	2.0	**6.26**	64.06	2.2	0.63	6.3	3.92	6.5	3.58	6.5
0.44	0	**2.37**	3.03	2.3	3.76	2.5	1.82	2.4	4.00	2.3
0.44	1.0	**4.18**	42.05	2.4	3.60	4.0	3.07	4.1	0.09	4.2
0.44	2.0	**5.80**	56.52	2.5	0.62	5.8	6.19	6.2	3.02	6.0
0.50	0	**1.40**	3.03	1.4	0.12	1.4	6.90	1.3	9.81	1.3
0.50	0.5	**1.99**	29.73	1.4	3.86	2.1	6.03	1.9	0.18	2.0
0.50	2.0	**4.59**	67.30	1.5	2.82	4.5	6.91	4.3	2.35	4.5
0.50	2.5	**5.43**	71.84	1.5	1.91	5.5	0.19	5.4	2.82	5.6

Table 4.3. *The table reports a summary of the error obtained after the application of the $P_3 - T_3$ method and its various upgrades. The first version is not reported, due to the fact it does not constitute a significant upgrade to the original model. In the third column, named REF., are listed the reference values of EINO$_x$, calculated through the 0D simulation presented in Sec. 3.3.*

augmenting the Mach, in first approximation is possible to consider it equal to 1 without committing any significant error.

- It is clear, also observing the behaviour of a, that the strongest contribute is given by the changing of the exponents b and c. Looking to the first variation in the graph, b alone still gives a big effort to the modeling, such as already the first approximation of the $P_3 - T_3$ gives an optimal interpolation. The influence of the parameter b is also considerable observing that it assumes values orde of magnitudes higher than the corresponding 0.4 in the original formulation.
  The motivation could lie in the different fuel: the hydrogen combustion is much more sensitive to the pressure than that of the kerosene, so the weight of its ratio

is higher.

- Analyzing the last and most complete approximation, the exponent c is taken in account, and its values at Mach 0.30 and 0.50 seems closer to 0, but the number of data is not enough to define a trend. Furthermore the markedly decreasing trend of b is no longer such.

4.2.2 Constant fuel-to-air ratio

In order to investigate the influence of the pressure ratio, the $P_3 - T_3$ method has been applied also to a new propulsive database computed through the upgraded model of the ATR keeping constant the equivalence ratio at value $\phi = 0.75$.

The set of new points is reported in Tab. 4.5.The first two columns represents the flight condition, the lasts three the output of the kinetic mechanism in term of temperature and pressure at the ignition and $EINO_x$.

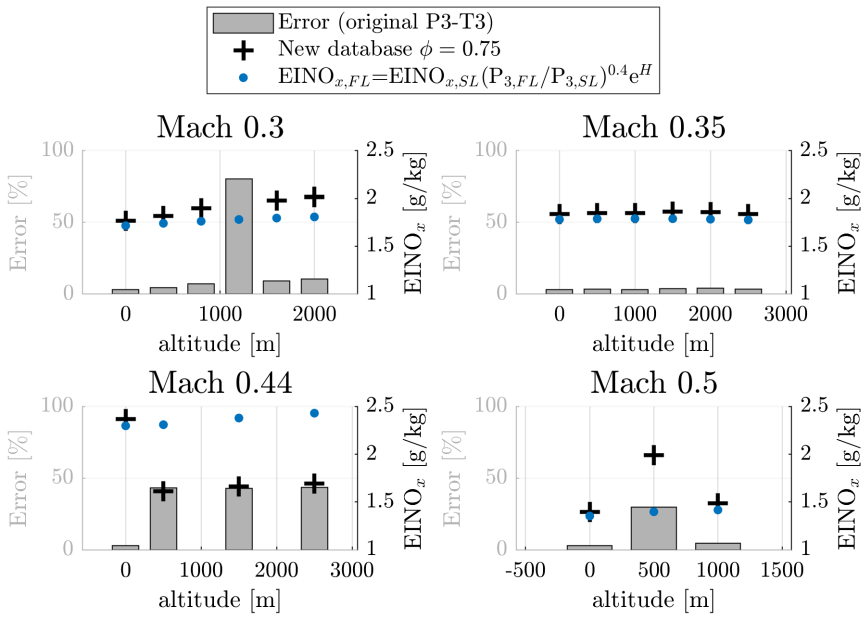

Figure 4.16. *Results of the application of the $P_3 - T_3$ method to a database with fixed equivalence ratio $\phi = 0.75$.*

The application of the original formulation of the $P_3 - T_3$ to the points calculated keeping the FAR constants, which results are reported in Fig. 4.16, leads to the following results: the emissions seems to be constant, so this could be considered as a confirmation that the fuel-to-air ratio strongly influences the NO_x production. The original method well fits the database indeed, except for some irregular points at Mach 0.3 and 0.4[1],so eventually a could be considered as close to 1.

[1]The irregularity in Mach 0.44 relies in the SL reference point, so it influences the prevision of the $P_3 - T_3$, which infact gives constant and aligned results.

NEW POINTS: OUTPUT OF ATR UPDATED MODEL

Mach	**Altitude**	**Pressure**	**AIR Temp.**	**FUEL Temp.**	**FUEL flow rate**	**AIR flow rate**	**Equivalence Ratio**
M	z	p_{71}	$T_{\text{air},71}$	$T_{\text{fuel},71}$	$\dot{m}_{\text{fuel}}$	$\dot{m}_{\text{air}}$	ϕ
$[-]$	[m]	[Pa]	[K]	[K]	[kg/s]	[kg/s]	$[-]$
0.30	0	1.84E+05	520	351	8.6	397.6	0.75
0.30	400	1.86E+05	534	354	8.3	380.8	0.75
0.30	800	1.86E+05	547	356	7.9	364.6	0.75
0.30	1200	1.86E+05	558	359	7.6	348.9	0.75
0.30	1600	1.86E+05	567	361	7.3	333.8	0.75
0.30	2000	1.85E+05	574	362	6.9	319.2	0.75
0.35	0	2.65E+05	583	393	10.1	463.8	0.75
0.35	500	2.49E+05	571	389	9.6	439.5	0.75
0.35	1000	2.35E+05	557	385	9.1	416.1	0.75
0.35	1500	2.21E+05	542	380	8.6	393.8	0.75
0.35	2000	2.08E+05	525	376	8.1	372.4	0.75
0.35	2500	1.95E+05	505	371	7.7	351.9	0.75
0.44	0	2.40E+05	390	441	13.6	588.7	0.75
0.44	500	2.32E+05	463	380	12.0	552.5	0.75
0.44	1500	2.33E+05	474	386	10.8	495.0	0.75
0.44	2500	2.30E+05	464	391	9.6	442.4	0.75
0.50	0	2.32E+05	380	377	14.4	662.6	0.75
0.50	500	2.51E+05	398	414	14.3	633.9	0.75
0.50	1000	2.45E+05	407	389	12.9	594.5	0.75

Table 4.4. *New points calculated through the updated ATR model, input to the kinetic mechanism and to the $P_3 - T_3$ method. The thermodynamic variables are to intend at the pre-combustion stage.*

NEW POINTS: RESOURCES OF CHEMICAL CALCULATION				
Mach	**Altitude**	**Tignition**	**P ignition**	**NO_x Emission Index**
M [-]	z [m]	T_3 [K]	P_3 [Pa]	$EINO_x$ [g/kg]
0.30	0	2410.211	1.05E+06	**1.77**
0.30	400	2410.297	1.04E+06	**1.82**
0.30	800	2410.396	1.03E+06	**1.90**
0.30	1200	2411.306	1.02E+06	**9.04**
0.30	1600	2412.545	1.01E+06	**1.98**
0.30	2000	2411.620	9.96E+05	**2.02**
0.35	0	2402.803	1.33E+06	**1.84**
0.35	500	2403.664	1.28E+06	**1.85**
0.35	1000	2403.975	1.22E+06	**1.85**
0.35	1500	2406.352	1.17E+06	**1.86**
0.35	2000	2407.779	1.12E+06	**1.86**
0.35	2500	2409.787	1.07E+06	**1.84**
0.44	0	2449.529	1.34E+06	**2.37**
0.44	500	2402.487	1.28E+06	**1.61**
0.44	1500	2403.631	1.26E+06	**1.66**
0.44	2500	2404.111	1.24E+06	**1.69**
0.50	0	2399.852	1.36E+06	**1.40**
0.50	500	2428.391	1.39E+06	**1.99**
0.50	1000	2399.128	1.37E+06	**1.49**

Table 4.5. *Output of the kinetic mechanism, that constitute the input to the $P_3 - T_3$ method.*

4.2.3 Design trajectory

Relying on the original database it is possible to extract some representative points, building up a simple trajectory in terms of Mach number at a specific altitude, reported in Tab. 4.6. With this expedient the $P_3 - T_3$ method could be applied to a more complex and representative case; Mach 0.3 as been considered as the sea level reference.

EINOx - Design Trajectory

Mach	**altitude**	**T ignition**	**p ignition**	**NOx Emission Index**
M [-]	z [m]	T_3 [K]	p_3 [Pa]	EINO$_x$ [g/kg]
0.30	0	2423.70	1.04×10^6	**2.12**
0.44	2000	2449.53	1.34×10^6	**2.37**
0.50	4500	2449.53	1.34×10^6	**2.37**
0.75	8000	2449.53	1.34×10^6	**2.37**
0.82	8921	2449.53	1.34×10^6	**2.37**

Table 4.6. *EINOx calculated along a realistic trajectory.*

In the realistic case the fitting is promising in term of R-square just taking the FAR ratio in account, considering the two variations of the $P_3 - T_3$ method in which the factor a, b and $c = 1$ and with a variable c. In the following table, the coefficients of the

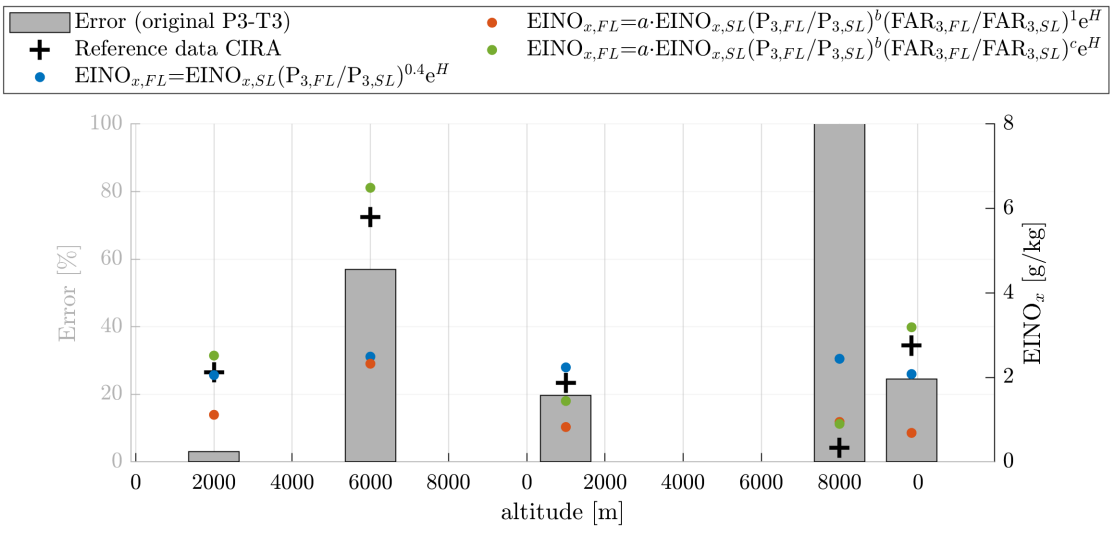

Figure 4.17. *Results of the application of the $P_3 - T_3$ method to a more realistic trajectory.*

fitting are reported: The coefficients reported in Tab. 4.7 are not in agreement with the trends identified before, but the points of the trajectory were not a lot and a more reliable result could be obtained deeply analyzing the real mission profile of STRAYOFLY. The evidence of a not direct applicability of the $P_3 - T_3$ method could reside in the fact that there is not a visible trend of the variables at sea level and the T_3; this could be due in turn

$P_3 - T_3$ VAR. 3		$P_3 - T_3$ VAR. 4		
a coeff.	**b** coeff.	**a** coeff.	**b** coeff.	**c** coeff.
~ 0.5	1.55	$\sim 1.$	-0.23	3.81

Table 4.7. *Factors found in the application of the variations of the $P_3 - T_3$ method to a more realistic trajectory.*

to the origin of the reference data, which arose from an optimization of the trajectory point per point and not from an engine model flying the whole mission. Analogously, the following path could consist in calculating a mission profile in term of required thrust based on the aerodynamic data present in literature about STRATOFLY, obtaining through the model the variables inside the engine for those points of the trajectory and base the calculation of the $P_3 - T_3$ method on a new database associated directly on the real mission.

The results in these terms could be easily compared with other applications and studies, such as the testing made on the SABRE engine mounted on Skylon performed in [9], in which a whole trajectory is analyzed and fitted. In his work the same variation to the $P_3 - T_3$ method has been implemented, and the results for the various fitting coefficients a , b and c are not even close to the values found applying the method at blocks at constant Mach number. In particular the value of a tend to reflect the more realistic case tried in this work, reported in Tab. 4.7. From the results indicated in the previous work also emerge the importance of the coefficient c, as long as the values found are a order magnitude higher than the results exposed in this section, underlining the importance of the fuel-to-air ratio over the pressure ratio, which exponent b found [9] is way different than its value computed here. These inconsistencies highlight the necessity to apply the $P_3 - T_3$, relatively to STRATOFLY, to a much realistic database.

Chapter 5

Conclusions and future works

The main scope of this thesis work was to experiment and value the applicability and the effectiveness of the $P_3 - T_3$ method, and eventually trying to upgrade it, with the aim to predicting the emissions of hydrogen fueled combined-cycle engines. In order to carry out this activity, the air turbo rocket designed on STRATOFLY was chosen as case study. To apply the method was necessary to compute several variables of ATR at sea level and at flight conditions, so a numerical model of propulsive system was developed.

5.1 Summary

In the first part of the work, after an introduction of the engine, the pre-existing model of ATR was analyzed and updated with the purpose to calculate the combustion variables and the performances of the engine. The influence of each upgrade was observed comparing the output of the model with a propulsive database computed by the von Kàrmàn Institute for Fluid Dynamics. As showed in the previous chapters, where all the results of the calculation are reported, the revision of the model gave different errors based on the flight conditions. The errors revealed a considerable adjustment for low Mach numbers and in the supersonic flight regime, while a mismatch is still present at high subsonic speed: considering Mach 0.30, the errors on thrust lowered from values higher than 100% to less than 10% and, at supersonic flight speeds, the error on the thrust output is on average lower than 10%.

The second part of the work was all about the evaluation of the emissions of ATR. The updated model was used to extend the propulsive database with the most suitable points at sea level, or to directly determine new sections. Hence the $P_3 - T_3$ method was chosen for its methodological approach to the prevision of the emissions, and it was considered the most suitable for this application. First was created an emissions database through the application of 0D chemical kinetic simulation to model the combustion. This database became the test bench to compare the results of the predictive method. The

canonical formulation of the $P_3 - T_3$ method seems to be not immediately applicable, and some specially adapted versions were tried: the accuracy improved significantly, with errors lower than 5%, and examining the formulation of the variants to the original method emerged some significant trend in the coefficients.

5.2 Future works

Concerning the model of the propulsion plant, it significantly improves the precedent, but some more updates could be implemented: for example an important step would be to build a model of the heat exchanger and put it in a loop to determine with more accuracy the temperature of the fuel entering in the combustion chamber. It is also possible to do several consideration regarding the intake, that should be modeled also in function of the altitude.

Regarding the prediction of the emissions, there are still some mismatches with the coefficients of the various declinations of the $P_3 - T_3$ method, and their physical meaning has to be deepened. More consideration about the coefficients of the reformulations and their trends could be done by applying the method to the design flight trajectory of the case study.

Bibliography

[1] Hiroshi Akima. “A New Method of Interpolation and Smooth Curve Fitting Based on Local Procedures”. In: *Journal of the ACM* (1970).

[2] J. A. Bossard and M. E. Thomas. “The Influence of Turbomachinery Characteristics on Air Turbo Rocket Engine Operation”. In: (July 2000). DOI: 10.2514/6.2000-3308.

[3] N. Chandrasekaran and Abhijit Guha. “Study of Prediction Methods for NOx Emission from Turbofan Engines”. In: *Journal of Propulsion and Power* (2012). DOI: 10.2514/1.B34245.

[4] Doug DuBois and Gerald C. Paynter. “"Fuel Flow Method2" for Estimating Aircraft Emissions”. In: (2006).

[5] Victor Fernàndez-Villacé. “Simulation, Design and Analysis of Air-Breathing Combined-Cycle Engines for High Speed Propulsion”. PhD thesis. Escuela Tecnica Superior di Ingenieros Aeronauticos, 2013.

[6] Davide Ferretto, Roberta Fusaro, and Oscar Gori. *Stratospheric Flying Opportunities for High-Speed Propulsion Concepts*. Restricted document/report. June 2018.

[7] Roberta Fusaro, Nicole Viola, and Diego Galassini. “Sustainable Supersonic Fuel Flow Method: an evolution of the Boeing Fuel Flow Method for supersonic aircraft using sustainable aviation fuels”. In: (2021). Ed. by Kostas Eleftheratos. DOI: doi.org/10.3390/aerospace8110331.

[8] D. G. Goodwin. “An open-source, extensible software suite for CVD process simulation, Chemical Vapor Deposition”. In: (Aug. 2003).

[9] Giovanni Grimaldi. “Development of a conceptual design tool to predict performance and pollutant and GHG emissions of high-speed vehicles using liquid hydrogen”. MA thesis. 2020.

[10] ICAO. *ICAO Annex 16: Environmental Protection, Volume II – Aircraft Engine Emissions*. 2008.

[11] ICAO. *ICAO website for combustion reports*. www.icao.int/envclq/CLQ07/Presentations/moran.pdf.

[12] Antonella Ingenito. "NO_x reduction strategies in scramjet combustion." In: *Aerospace Science and Technology* (2016). DOI: 10.1016/j.ast.2016.10.020.

[13] Marlene Johansson. *NOx Emissions and Engine Performance Results for Studied Engine Concepts including final summary*. 2010.

[14] MathWorks®. *Coefficient of Determination (R-Squared)*. https://it.mathworks.com/help/stats/coefficient-of-determination-r-squared.html. 2022.

[15] Christophe Meerts and John Steelant. "Air Intake Design for the Acceleration Propulsion Unit of the LAPCAT-MR2 Hypersonic Aircraft". In: EUCASS (July 2013). DOI: 10.2139/ssrn.2277103.

[16] Simone Moino. "Methodology and tools for propulsive performance characterization of high-speed aircraft in conceptual design". MA thesis. 2020.

[17] Guido Saccone. *CIRA contribution to Updates on STRATOFLY MR3 emissions*. Restricted document/report. June 2020.

[18] Martin Schaefer. "Methodologies for Aviation Emission Calculation - A comparison of alternative approaches towards 4D global investors". MA thesis. 2006. DOI: 10.14279/depositonce-1476.

[19] N. N. Smimov and V. F. Nikitin. "Modeling and simulation of hydrogen combustion in engines". In: *International Journal of Hydrogen Energy 39(2014)* (2014). Ed. by Emre A. Veziroglu.

[20] Stratofly-H2020. *STRATOFLY: Stratospheric Flying Opportunities for High-Speed Propulsion Concepts*. https://www.h2020-stratofly.eu/. 2018.

[21] Nobuhiro Tanatsugu, Tetsuya Sato, and Yoashihiro Naruo. "Development Study on ATREX Engine". In: (1997).

[22] L. Trainelli. *Lezioni di Meccanica del Volo*. 2011.

[23] J. Warnats, U. Maas, and R. W. Dibble. *Combustion: Physiscal and Chemical Fundamentals, Modeling and Simulation, Experiments, Pollutant Formation*. Springer, 2006. ISBN: ISBN-10 3-540-25992-9.

[24] N. Zettervall and C. Fureby. "Computational Study of Ramjet, Scramjet and Dual Mode Ramjet/Scramjet Combustion in a Combustor with a Cavity Flameholder". In: (2018).